# Establishment of a wireless charging system for a battery-operated automatic guided vehicle

presented by

**Andrè Llewellyn Pawson**

Thesis submitted in fulfilment of the requirements for the degree

**MASTERS of ENGINEERING in ELECTRICAL ENGINEERING**

in the

**Department of Electrical, Electronic and Computer Engineering**

of the

**Faculty of Engineering and Information Technology**

at the

**Central University of Technology, Free State**

Promoter: Prof HJ Vermaak, PhD

Bloemfontein

November 2018

# Declaration

I, ANDRè LLEWELLYN PAWSON, identity number and student number , do hereby declare that this research project which has been submitted to the Central University of Technology Free State, for the degree MASTERS of ENGINEERING in ELECTRICAL ENGINEERING, is my own independent work and complies with the Code of Academic Integrity, as well as other relevant policies, procedures, rules and regulations of the Central University of Technology, Free State, and has not been submitted before by any person in fulfilment (or partial fulfilment) of the requirements for the attainment of any qualification.

SIGNATURE OF STUDENT

10 October 2018
DATE

# Acknowledgements

I would like to thank the following persons and institutions for their unselfish assistance and support during the research project:

My promotor, Prof. Herman Vermaak, for his guidance and assistance during the research period; and Dr Ben Kotze for his contribution to the final product.

Central University of Technology, Free State for the indirect help and support that made my studies possible.

The Research Group in Wireless Power Transfer Technology for the equipment, time, effort and assistance throughout the research period. Ricus Cox, Teboho Ntsinyi, Gareth Gericke and Nathan Walbrugh for getting the research at CUT on this topic started by doing relevant individual projects on related topics.

My colleagues, Dr Nicolaas Luwes, Johan Raath and Rion Pretorius for exchanging thoughts, ideas and support towards the completion of this study.

Finally, and especially my wife, Adri, and my daughter, Anri, for their love and support during the long period of study.

# Abstract

Modern technology provided a requirement that more power systems are being replaced with automated systems. Automatic Guided Vehicles (AGV) are Electric Vehicles (EV) that make use of re-chargeable batteries as a power module in the automation process. The increase in use of an AGV requires an essential method that is safe, quick and convenient to recharge the system. Wireless transfer technology has become an effective and reliable option to replace the conventional wire transfer technology. The topology involves a power transmitter assembled to the grid, and a power receiver assembled to the battery. A wireless power transfer system should satisfy three conditions, namely high efficiency, large air gaps and high power. Recent studies have provided wireless mid-range charging technology to transfer power through resonant inductive coupling.

The theory of resonant inductive coupling will therefore be used as the main technology in the design and implementation of a wireless charging system that can be successfully implemented with AGVs. The intention is to be able to wirelessly transform and transfer an alternating oscillating waveform into a DC voltage, to demonstrate instantaneous power transfer. To improve the comprehension on the theories related to “Magnetic Resonant Coupling”, quality factor and optimisation techniques of wireless power transfer systems, a design will be presented, along with the working principles and constructions of various components.

# Table of Contents

Declaration ..... ii

Acknowledgements ..... iii

Abstract ..... iv

List of Figures ..... vii

**1 Preface** **1**

1.1 Introduction ..... 1

1.2 Problem statement ..... 3

1.3 Purpose of study ..... 3

1.4 Hypothesis ..... 4

1.5 Specific objectives ..... 4

1.6 Expected outcomes ..... 5

1.7 Limitations of study and future research ..... 5

1.8 Outlines of the dissertation ..... 5

**2 Wireless transfer of electrical energy** **7**

2.1 Introduction ..... 7

2.2 Field of study ..... 9

2.2.1 Direct induction ..... 10

2.2.2 Resonant magnetic induction ..... 16

2.2.3 Electromagnetic radiation ..... 22

**3 Wireless power transfer system** **26**

3.1 Introduction ..... 26

3.2 Design of the wireless power system ..... 27

3.2.1 Oscillator ..... 28

3.2.2 Power amplifier ..... 32

3.2.3 Transmitter and receiver coil configuration ..... 33

3.2.4 Composition of the inductance of a coil ..... 34
3.2.5 Voltage rectifier ..... 34
**4 Experimental set-up and results 36**
4.1 Experimental procedures for optimum coil configuration ..... 36
4.1.1 Evaluation for optimum coil configuration..... 45
4.1.2 Experimental test set-up..... 49
4.1.3 Final test set-up and recorded results..... 51
**5 Conclusion 65**
5.1 Wireless power transmission..... 65
5.2 Future work ..... 66
5.3 Applications..... 67
**6 References 69**

# List of Figures


Figure 2.1 Typical arrangement of an inductively coupled power transfer system [2]. 11

Figure 2.2 Power efficiency for an inductive power transfer system, consisting of loop inductors in dependence on their axial distance z with size ratio as parameter. Calculated for a quality factor of Q=100 [5]. ..... 14

Figure 2.3 Lowest system loss factor as a function of the FOM (figure of merit) [5]... 16

Figure 2.4 Magnetic coupling that links the two circuits ..... 17

Figure 2.5 Equivalent circuit of magnetic resonant coupling ..... 18

Figure 2.6 Coupled model with capacitor $C_s$ ..... 20

Figure 2.7 Equivalent primary circuit model including the reflected impedance ..... 20

Figure 2.8 Electromagnetic waves ..... 23

Figure 3.1 Block diagram of the wireless power transfer system ..... 27

Figure 3.2 Configuration of the Hartley oscillator ..... 29

Figure 3.3 A typical Colpitts oscillator with a transistor on which our design will be based ..... 31

Figure 3.4 Switch-mode amplifier ..... 33

Figure 3.5 Normal full wave bridge rectifier ..... 35

Figure 4.1 Single-layer helix (a) Single-layer flat spiral (b) Multi-layer spiral (c) ..... 37

Figure 4.2 A single-layer helix coil drawn in FEMM software ..... 38

Figure 4.3 The flux density and magnetic lines of a single-layer helix coil, represented as a colour density plot ..... 38

Figure 4.4 The flux density and magnetic lines of a single-layer helix coil, horizontal to the coil ..... 39

Figure 4.5 The graph shows the distance versus the magnetic field strength in Tesla .. 40

Figure 4.6 The flux density and magnetic lines of a single-layer helix coil, vertical to the coil ..... 40

Figure 4.7 The graph shows the magnetic field strength versus distance ..... 41

Figure 4.8 A single-layer flat spiral coil drawn in FEMM software ..... 42

Figure 4.9 The black lines are an indication of the magnetic flux lines when current flows through the coil ..... 42

Figure 4.10 The flux density and magnetic lines of a single-layer flat spiral coil, vertical to the coil ..... 43
Figure 4.11 The graph shows the distance versus the magnetic field strength in Tesla .. 43
Figure 4.12 The flux density and magnetic lines of a single-layer flat spiral coil, horizontal to the coil ..... 44
Figure 4.13 The graph shows the distance versus the magnetic field strength of the horizontal line ..... 44
Figure 4.14 Efficiencies of the three coil configurations ..... 46
Figure 4.15 Maximum power transfer point or resonant frequency point ..... 47
Figure 4.16 Alignment effect between the two coils ..... 48
Figure 4.17 Experimental set-up with Multisim software ..... 49
Figure 4.18 Primary coil on laminated core ..... 52
Figure 4.19 Secondary coil on laminated core ..... 53
Figure 4.20 Hardboard mould with 5 mm increments for the coils ..... 54
Figure 4.21 Recorded variation of inductance of coil A ..... 55
Figure 4.22 Recorded variation of inductance of coil B ..... 56
Figure 4.23 Practical test set-up with coils 100 mm apart and no load ..... 57
Figure 4.24 Recorded DC voltage at coils 100 mm apart with no load ..... 58
Figure 4.25 Calculated current with coils at 100mm and load of 10 kΩ ..... 59
Figure 4.26 Recorded DC voltage at coils 50 mm apart with no load ..... 61
Figure 4.27 Calculated current with coils at 50 mm and load of 10 kΩ ..... 62
Figure 4.28 Recorded DC voltage at coils at 10 mm apart with no load ..... 63
Figure 4.29 Calculated current with coils at 10 mm and load of 10 kΩ ..... 64

List of Tables

Table 4.1 Output voltage versus distance configurations ..... 50
Table 4.2 Primary and secondary coil specifications ..... 52
Table 4.3 Inductance test on both coils at 1 kHz sine wave ..... 55
Table 4.4 Recorded test results with coils 100 mm apart and no load ..... 57
Table 4.5 Recorded test results with coils 100 mm apart and a 10 kΩ load resistor .... 59
Table 4.6 Recorded test results with coils 50 mm apart and no load ..... 60
Table 4.7 Recorded test results with coils 50 mm apart and a 10 kΩ load resistor ..... 61
Table 4.8 Recorded test results with coils 10 mm apart and no load ..... 62
Table 4.9 Recorded test results with coils 10 mm apart and a 10 kΩ load resistor ..... 63

Chapter 1

# Preface

*This chapter provides an overview of the proposed research problem, aim, methodology, and hypothesis, with the chapter layout necessary to design, test and implement a wireless charging system for an Automatic Guided Vehicle that will reduce the operational and maintenance costs related to the unavailability of AGVs.*

## 1.1 Introduction

An automatic guided vehicle (AGV) is a mobile robot that is guided by machine vision, lasers, markers or wires in the floor. They are widely used in industrial applications for the conveyance of materials around a manufacturing facility or a warehouse. The use of these automatic guided vehicles has increased in the past few years.

Optimum profitability of these AGVs requires a high utilisation factor, therefore the recharging of the batteries of these vehicles normally presents a problem.

Several different battery charging options are utilised by AGVs. The different options depend on the user's preference. The most commonly used battery charging technologies are *Battery Swap*, *Opportunity Charging* and *Automatic Battery Swap*.

*"Battery swap technology"* requires an individual to manually remove the discharged battery from the AGV, and to replace it with a fully charged battery, approximately every 8 – 12 hours, or about one working period. This is a time-consuming action that lasts for about 5 – 10 minutes, and is performed with each AGV in the fleet.

*"Opportunity battery charging"* allows for continuous operation. The average automatic charging procedure for an AGV is equal to 12 minutes every hour. With opportunity charging the AGV will receive a charge whenever the opportunity arises. When the battery of the AGV reaches a specific level, it will complete the operation that it has been assigned, and will then proceed to the charging station.

*"Automatic Battery Swap"* is an alternative to manual battery swap technology. It requires additional automated machinery in the form of an automatic battery changer, whereby the AGVs will proceed to the battery swapping station and have their batteries automatically replaced with fully charged batteries. The discharged batteries will then automatically be placed into a charging slot for automatic recharging. An additional feature of this process is that the automatic battery changer records the charging time of every battery to ensure that the system will complete the replacement with a fully charged battery.

Automatic battery swap technology reduces the manpower required, but recent developments in battery charging technology allow for quick and efficient charging regimes that potentially eliminates the need to swap batteries.

## 1.2 Problem statement

Opportunity charging of AGVs are more widely used than any of the other charging regimes, and makes use of a charging stations that are strategically placed within the system to allow the efficient operation of the production process. The current charging technology comprises a battery charging contact that usually consists of a base plate, which is installed on the floor or laterally with a bracket adjacent to the AGVs runway, and a current collector which is installed on the vehicle. Once the AGV is in the charging position, and the collector has made contact with the base plate, the charging procedure starts.

It is therefore safe to conclude that if physical contact is not completed between the current collector and the base plate, the charging process will be at risk. It is also obvious that this system makes use of normal electrical wiring through contacts to complete the charging process. Hence, maintenance of the system will be an issue. It is therefore evident that the introduction of wireless charging technology or "WiTricity", as it is commonly known, will improve the charging process comprehensively [1].

## 1.3 Purpose of study

The purpose of this research is to establish a wireless charging technology that is best suitable for battery-operated automatic guided vehicles.

The expected outcome of the research is therefore to:

- identify the best wireless charging technology;
- introduce and develop this technology for AGVs;

- recommend actions to improve AGV operation, due to limited battery capacity;
- establish a wireless AGV charging system; and
- substantially reduce maintenance and operational related costs.

## 1.4 Hypothesis

It is considered possible to compile relevant technical information regarding wireless charging technologies that could positively affect the operational efficiency of a battery-operated AGV.

It is also considered possible to establish an improved system which could assist and enhance the use of AGVs in the production cycle, without removing the AGV from the production process.

## 1.5 Specific objectives

This research project aims to achieve the following:

- design, test and implement an expert wireless charging system for a National Instruments AGV platform with a 3000 mAh Nickel Metal Hydrate battery, charged at 0.9 A ; and
- to reduce operational and maintenance costs related to unavailability of AGVs.

## 1.6 Expected outcomes

The expected outcomes of the research are:

- the completion of a wireless charging system that can be successfully implemented with the AGVs, used at the Central University of Technology, Free State (CUT); and
- to reduce the operational and production costs related to the availability of an AGV.

## 1.7 Limitations of study and future research

The wireless charging system will only address the actual charging configuration, and will therefore exclude any work on the type of batteries that could enhance the efficiency of the overall system.

## 1.8 Outlines of the dissertation

The theory of direct induction, resonant magnetic induction and electromagnetic radiation will be covered in Chapter 2 to establish the main technology in the design and implementation of a wireless charging system that can be successfully implemented with AGVs. The objective of Chapter 3 is to obtain the most effective coil configuration, and to design and implement a system to show the development process of all the components that configure a “Wireless power transfer system”. In Chapter 4, the results of the experimental test set-up will be completed to establish the optimum coil configuration for a resonant wireless power transfer system. In

Chapter 5 the results obtained will be discussed, with some recommendations made on how such a system can be improved.

Chapter 2

# Wireless transfer of Electrical Energy

*This chapter gives an overview of the proposed systems necessary to transfer power wirelessly. "WiTricity", or wireless energy transmission, is the process of transmitting electrical energy from a power source to an electrical load, without using any conducting material. Wireless transmission is widely accepted in cases where the use of any physical contact becomes inconvenient, hazardous or impossible* [1].

## 2.1 Introduction

The term "WiTricity" originated in the year 2007, with a project that was initiated by Marin Soljacic at MIT [1]. The researchers at this institution successfully demonstrated the electrification of a 60 W light bulb without any conductors connected between the supply and the load. The experiment made use of two five-turn copper coils that was spaced two meters apart, and with a diameter of 60 cm. The coils, designed to resonate together at 9.9 MHz and oriented along the same axis, obtained an efficiency of roughly 45 %. The one coil was inductively connected to a power source, whilst the other coil was connected to the load or 60 W light bulb. The result of this experiment was that the bulb was powered, even though the direct line of sight was blocked by a wooden panel. In addition to this, the researchers were able to power the same load at roughly 90 % efficiency at a distance of 0.91 m.

The wireless transfer of energy, WiTricity, is based on a very strong coupling between resonant electromagnetic objects, which differs from other methods used,

such as induction microwaves, or ionisation of air particles [1]. This system normally comprises transmitters and receivers that contain magnetic loop antennas that are critically tuned to similar frequencies. The attainment of this electromagnetic near-field technology depends on the fact that the receiving devices should not be further than a quarter wave length from the transmitting units.

The wireless charging devices are connected almost entirely with magnetic fields, largely confined in capacitors within the devices, which arguably makes them safer than resonant energy transferring devices that uses electric fields, similar to Tesla coils. WiTricity devices are also known to be unusual in that they support efficient energy transfer in “mid-range” distances that are several times larger than the diameter of the resonant object [1].

WiTricity employs near-field resonant inductive coupling through magnetic fields, similar to those found in transformers, which are unlike the far-field wireless power transmission systems that are based on traveling electromagnetic waves [1]. The exception is that the primary coil and secondary windings are physically separated and tuned to resonate in order to increase the magnetic coupling between them. The tuned magnetic fields that are generated by the primary coil can be controlled to vigorously interact with the matched secondary windings, detached from the primary coil. The basic principle of WiTricity is to use “strongly-coupled” resonances, in order to achieve high power transfer efficiency [1].

## 2.2 Field of study

Wireless power transmission differs from wireless telecommunications in the sense that with radio the proportion of energy received from the transmitter should not become too low for the signal to be distinguished from the background noise, whilst with wireless power transmission, the efficiency is the more significant parameter. In order to ensure an economical system, it is imperative that a large part of the energy that was sent out by the transmitter should be received by the load [2].

The technology of wireless power transfer is applicable in a variety of applications and environments, and will improve the products produced. Wireless power transfer can be applied in two different modes, namely:

**Direct wireless power:**

No batteries are used, and therefore all the power that the device needs will be supplied directly from the power source. The disadvantage of this system is that the device should always be within the charging range of the power source.

**Automatic wireless charging:**

In this mode the rechargeable batteries of the device will be charged whilst the device is operational or stationary, without the need of a power cord or a battery replacement. The advantage of this mode is that the mobile device is not restricted to the range of the power source.

The most widely used form of WiTricity is the use of direct induction followed by resonant magnetic induction [1]. Electromagnetic radiation that comprises microwaves or lasers, is also considered as a method of wireless power transfer.

### 2.2.1 Direct induction

Electromagnetic induction is directly proportional to the strength of the voltage, current and frequency of the magnetic field. The greater the frequency, the higher the induction effect becomes. Energy will be transmitted from the conductor that produces the primary field to any secondary conductor that is within this field. A high frequency current will not induce over long distances, but will transfer a great amount of energy through the field to any adjacent conductor. Increased induction due to a higher frequency can be compared to the apparent difference between the transfer of high frequency disturbances, and the transfer of low frequency power in alternating current systems. An increased frequency will lead to a more preponderant inductive effect that causes the transfer of energy between adjacent circuits in space, while a rapid decrease in the current will lead to a decrease in energy transfer and the more local will the phenomenon become.

The transfer of electric energy thus consists of a phenomenon inside a conductor, and the phenomena in the space outside the conductor. The electric field, on the other hand, is a steady magnetic and dielectric stress in a continuous current circuit, compared to an alternating field with an alternating current in the conductor that produces an electric wave that becomes far-field electromagnetic radiation traveling through space at the speed of light.

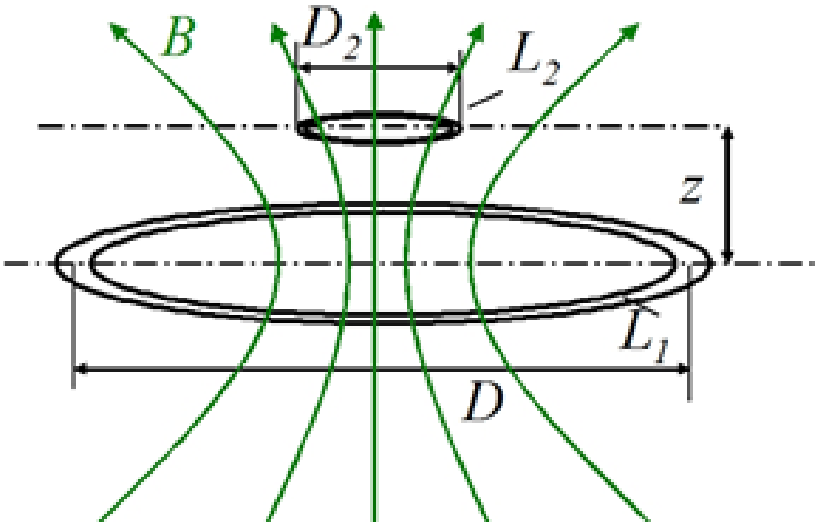


**Figure 2.1 Typical arrangement of an inductively coupled power transfer system [2].**

Figure 2.1 shows the principle of an inductively coupled power transfer system. The circuit consists of a transmitting coil (L1) and a receiving coil (L2) that forms magnetically coupled inductors. A changing flux in L1 generates a magnetic field that induces a voltage in L2. The voltage generated in the receiving coil can be used to charge a secondary device or a battery. The charging efficiency is determined by the coupling coefficient (k) and quality factor (Q) that exists between the two coils [3].

The general definition of the quality factor is based on the ratio of the apparent power to the power losses that exist in the coil, hence the quality factor Q of a coil can be calculated as follows:

$$Q = \frac{\omega L}{R} \tag{1}$$

The quality factor is a dimensionless parameter that describes the characteristics of an oscillator or resonator, or equivalently, characterizes a resonator's bandwidth,

relative to its centre frequency. A higher Q-factor indicates the stored energy of the oscillator is relative to a lower rate of energy loss and slower fading of the oscillations. Sinusoidal signal driven resonators with high Q-factors normally resonate with greater amplitudes at resonant frequencies, but have a smaller range of frequencies around that frequency for which they resonate at. The range of frequencies for which the oscillator resonates, is called the bandwidth. The quality factor for a fixed operating frequency mainly depends upon the shape and size of the coil, as well as the materials used.

The coupling coefficient is determined by the distance between the coils (z), the ratio of $D_2/D$, and furthermore by the shape of the coils as well as the angle between them. The definition of the coupling coefficient k is given by:

$$k = \frac{L_{12}}{\sqrt{L_{12}.L_{22}}} \tag{2}$$

This equation results from the general equation system for coupled inductors,

$$\frac{U_1}{j.\omega} = L_{11}.I_1 + L_{12}.I_2 \tag{3}$$

$$\frac{U_2}{j.\omega} = L_{12}.I_1 + L_{22}.I_2 \tag{4}$$

Where,

$U_1$ and $U_2$ = voltages applied to the coils

$I_1$ and $I_2$ = currents measured in the coils

$L_1$ and $L_2$ = self-inductances

$L_{12}$ = the coupling inductance

The coupling coefficient, k, can now be determined as follows:

$$u = \frac{U_2}{U_1} = k\sqrt{\frac{L_2}{L_1}} \quad (5)$$

The optimal calculated efficiency of such a system, with an assumed quality factor of a 100, is shown in Figure 2.2. The dimensions of these calculations have been scaled to the diameter of the larger coil (D). The values reflected are shown as a function of the axial distance of the two coils (z/D), while the variable value used, is the diameter of the smaller coil $D_2$ [4].

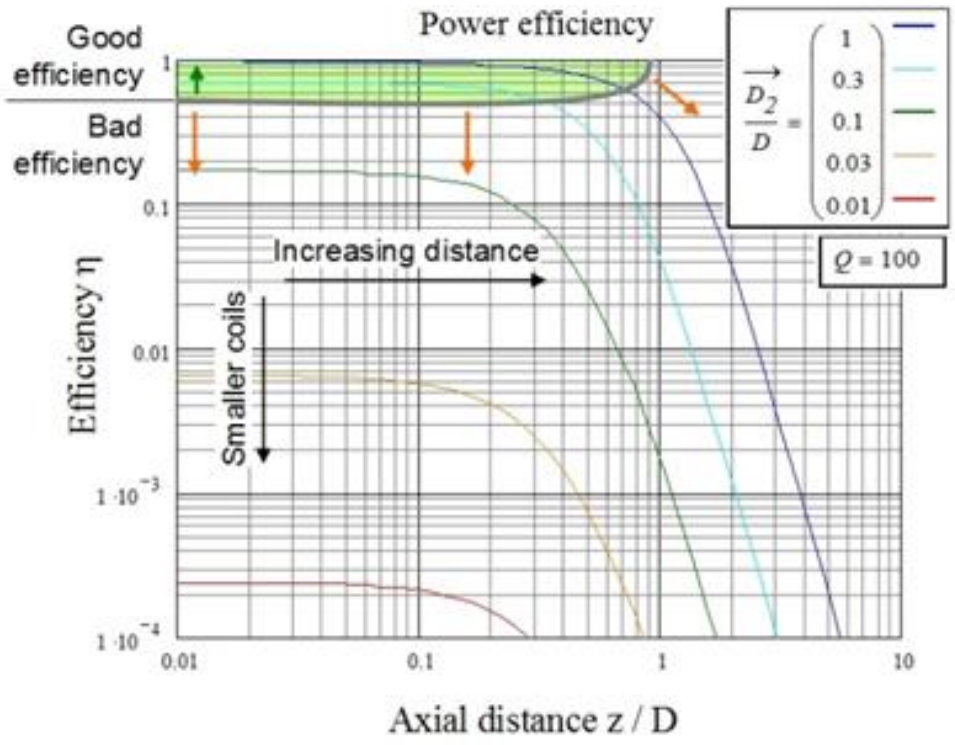


**Figure 2.2 Power efficiency for an inductive power transfer system, consisting of loop inductors in dependence on their axial distance z with size ratio as parameter. Calculated for a quality factor of Q=100[5].**

The graph shows that at larger distances (z/D > 1), or at a large size difference of the coil ($D_2/D < 0.3$), the efficiency is reduced drastically. It also shows that a high efficiency (> 90 %) can be achieved at reduced distances (z/D < 0.1), as well as for coils of similar sizes ($D_2/D = 0.5$). Therefore, it can be concluded that direct inductive power transmission across large distances into space is very inefficient.

The losses that appear in a wireless system will limit the power transfer of the system. All these losses related to the transferred power, can be expressed as a loss factor with the following equation:

$$\lambda = \frac{P_{Loss}}{P_{Out}} \tag{6}$$

A deeper analysis of the loss factor shows that with a properly matched generator and load, the minimum loss factor can be achieved, as indicated in the equation below:

$$\lambda_{Min=\frac{2}{(kQ)^2}.(1+\sqrt{1+(kQ)^2})} \quad (7)$$

The equation shown graphically in Figure 2.3 depends on the basic parameters of a wireless inductive system. These parameters are the coupling factor k, which exists between the receiving and transmitting coils, and the quality factor Q, of the system. The geometrical average of the transmitter and receiver's quality factors produces the quality factor of the system. The equation indicates that the product of the system quality factor Q and the coupling factor k, are directly proportional, and therefore a poor coupling factor could be compensated for by a better-quality factor, and vice versa.

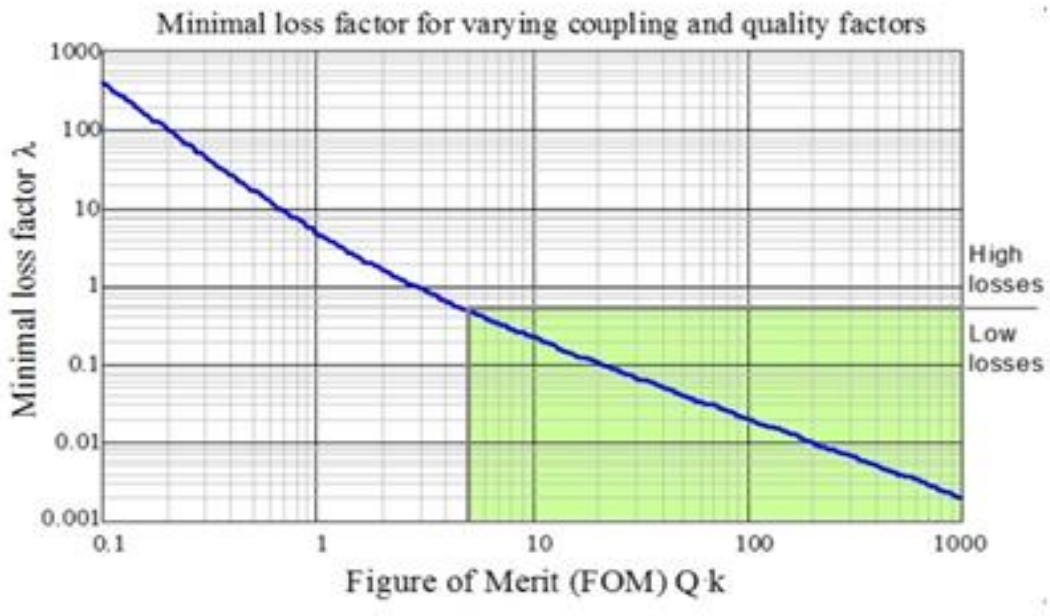


**Figure 2.3 Lowest system loss factor as a function of the FOM (figure of merit) [5].**

### 2.2.2 Resonant magnetic induction

The wireless transmission of electrical energy in the near field, between two coils that are tuned to resonate at the same frequency, is known as "resonant inductive coupling". The coupling works on the principle of electromagnetism. In the field of wireless power transfer, magnetic coupling is an old and well understood method. Although the quick decay of the magnetic field limits the effective distance, the power transfer can be enhanced by applying resonance with the magnetic coupling. This also achieves at a greater distance, compared to no resonance.

The equivalent circuit that represents the magnetic coupling is shown in Figure 2.4. A circuit is magnetically coupled when a portion of the magnetic flux established by a circuit, and links with another circuit to transfer energy from the one to the other. The transfer of energy is performed by the magnetic field, which is common to both the circuits.

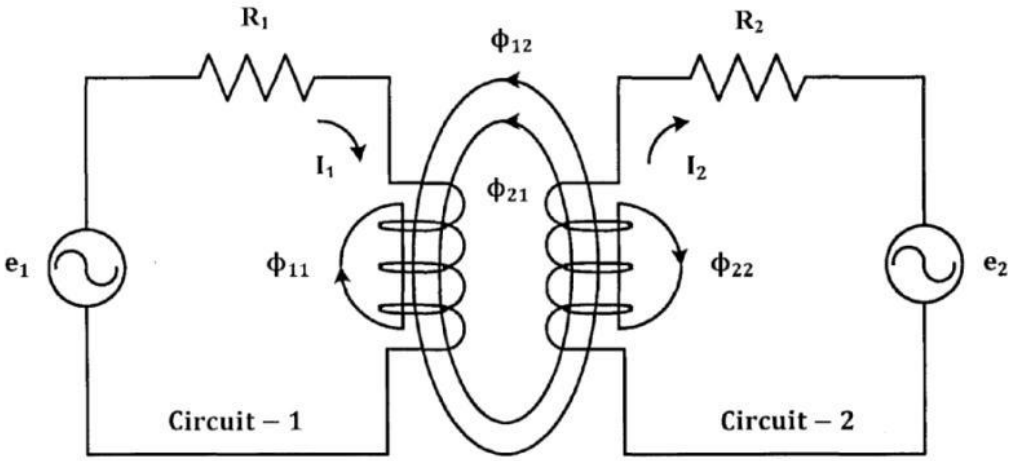


**Figure 2.4 Magnetic coupling that links the two circuits**

Inductive or magnetic coupling is based on the principle of electromagnetism. The magnetic flux established by $I_1$ can be divided into two components, $\Phi_{11}$ that links with the first circuit and not the second, and $\Phi_{12}$ that links with both the circuits. Similarly, the magnetic flux established by $I_2$ also consists of two components, namely $\Phi_{22}$ that links with circuit 2, but not with circuit 1, as well as $\Phi_{21}$ that links with both the circuits. This results in the following two equations:

$$\phi_1 = \phi_{11} + \phi_{12} \tag{8}$$

$$\phi_2 = \phi_{22} + \phi_{21} \tag{9}$$

The phenomenon of magnetic coupling that takes place between circuits is a result of $\Phi_{12,}$ the mutual flux produced by the first circuit, and $\Phi_{21,}$ the mutual flux produced by the second circuit. Coupling can be magnified or amplified by coiling the conductor, while power transfer can be increased by increasing the number of coils, strength of the current, cross-section of the coil and the strength of the radial magnetic field [6].

Resonant magnetic coupling is based on the same principles as inductive coupling, but applies resonance in order to increase the range at which energy transfer can efficiently occur.

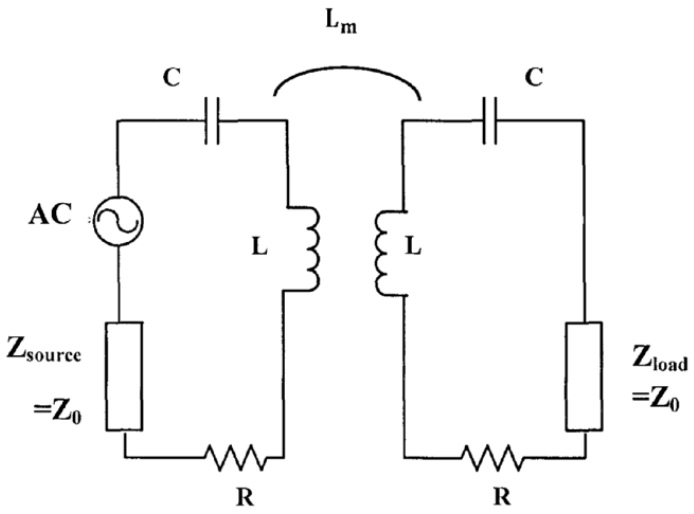


**Figure 2.5 Equivalent circuit of magnetic resonant coupling**

Energy transfer will occur between the primary and the secondary circuits, as shown in Figure 2.5. Primary particular resonance will occur when the primary current is in phase with the input voltage, while secondary particular resonance will take place when the secondary current is in phase with the induced voltage. Full resonance occurs when both the primary and the secondary circuits are in a resonant condition.

A resonant or resonance transformer, with a high Q value and an air core, in order to avoid losses, is normally used to accomplish this electrical energy transfer. The two coils could be a single piece of equipment, or it could be two separate pieces. Resonant transfer is reached by producing a ringing coil with an oscillating current, which produces an oscillating magnetic field. The fact that the coil is highly resonant, means that the energy developed in the coil will decrease relatively slowly over a number of cycles, unless an additional coil is introduced, even at some

distance from the first one, in order to absorb most of the energy before it is lost. The resonant frequency can be calculated from the equivalent circuit, and it would show that to satisfy the resonant condition, the reactance in Figure 2.5 has to be zero, as indicated in equation 10. Two resonant frequencies will satisfy the resonant condition shown in equation 10, and can be calculated as shown in equations 11 and 12.

$$\frac{1}{\omega L_m} + \frac{2}{\omega(L-L_m)\frac{1}{\omega C}} = 0 \tag{10}$$

$$\omega_m = \frac{\omega_0}{\sqrt{(1+K)}} = \frac{1}{\sqrt{(L+L_m)C}} \tag{11}$$

$$\omega_e = \frac{\omega_0}{\sqrt{(1+K)}} = \frac{1}{\sqrt{(L-L_m)C}} \tag{12}$$

$$K = \frac{L_m}{L} = \frac{\omega_e^2-\omega_m^2}{\omega_e^2+\omega_m^2} \tag{13}$$

The coupling coefficient (K), as indicated in equation 13, represents the strength of the magnetic coupling between the two coils, and can be calculated from equation 11 and 12. K is also closely related to factors such as the air gap between the two coils, as well as obstacles between them [7].

A tool that can be used to analyse the resonant coupling is the use of the calculated "reflected impedance". The circuit that is shown in Figure 6 shows the coupled model with capacitor $C_s$, added in series with the secondary winding to form a resonant circuit. $R_p$, $L_p$, $R_s$ and $L_s$ are the resistance and inductance of the primary

and secondary windings, respectively. M is the mutual inductance between the two circuits. The equivalent resistance of the load is represented by RL.

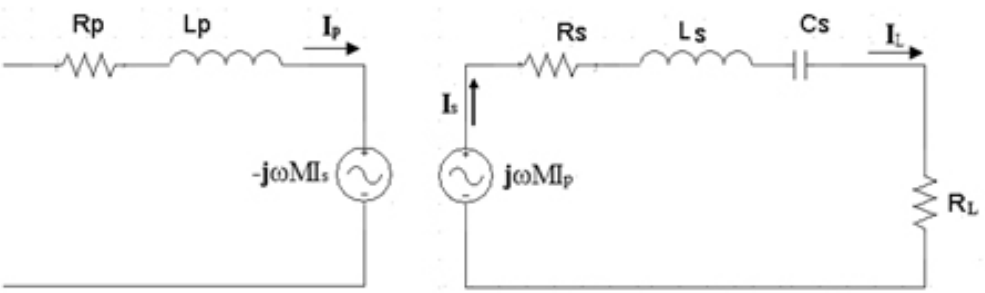


**Figure 2.6 Coupled model with capacitor $C_s$**

The equivalent model of the primary circuit that includes the reflected impedance is shown in Figure 2.7.

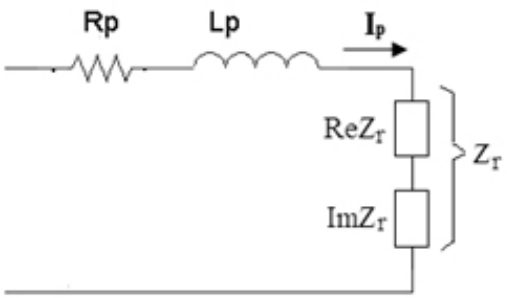


**Figure 2.7 Equivalent primary circuit model including the reflected impedance**

The reflected impedance, $Z_r$, consists of the real component, $ReZ_r$, and the imaginary component, $ImZ_r$, and can be expressed by the following two equations:

$$ReZ_r = \frac{\omega^4 C_S^2 M^2 (R_S + R_L)}{(\omega^2 C_S L_S - 1)^2 + \omega^2 C_S^2 (R_S + R_L)^2} \quad (14)$$

$$I_m Z_r = \frac{-\omega^3 C_S M^2 (\omega^2 C_S L_S - 1)}{(\omega^2 C_S L_S - 1)^2 + \omega^2 C_S^2 (R_S + R_L)^2} \quad (15)$$

The real component $ReZ_r$ of the reflected impedance needs to be maximised to increase the primary efficiency. When the two equations are analysed, it will show that, when the secondary circuit is operating under resonant conditions, as indicated by the following equation,

$$\omega = \frac{1}{\sqrt{C_S L_S}} \quad (16)$$

the reflected resistance or real component exhibits the maximum property, and is equal to the value determined by the following equation:

$$\frac{\omega^2 M^2}{R_L + R_S} \quad (17)$$

It will be found that the real component, $R_eZr$ can further be increased, by increasing the frequency, mutual inductance or by reducing the load resistance and secondary winding resistance. It should be noted, however, that a substantial reduction in the load resistance may influence the secondary efficiency, which equals the value determined by the following equation:

$$\frac{1}{1 + \frac{R_S}{R_L}} \quad (18)$$

Other resonant topologies, such as parallel resonance or a combination of series and parallel resonant combinations may be employed at the secondary side to obtain optimal operating conditions [8].

### 2.2.3 Electromagnetic radiation

Electromagnetic radiation (EMR) is an energy form produced by oscillating electric and magnetic fields, or by electrically charged particles that are travelling through vacuum or matter. The electric and magnetic fields move at right angles with each other, as shown in Figure 6, while the combined wave travels perpendicular to both oscillating fields, thus creating the disturbance. Electron radiation in the form of photons are released and consists of bundles of light energy, travelling at the speed of light as quantised harmonic waves. This energy is then combined into groups based on the wavelength in the electromagnetic spectrum. The electric and magnetic waves have certain characteristics, including amplitude, wavelength and frequency [4].

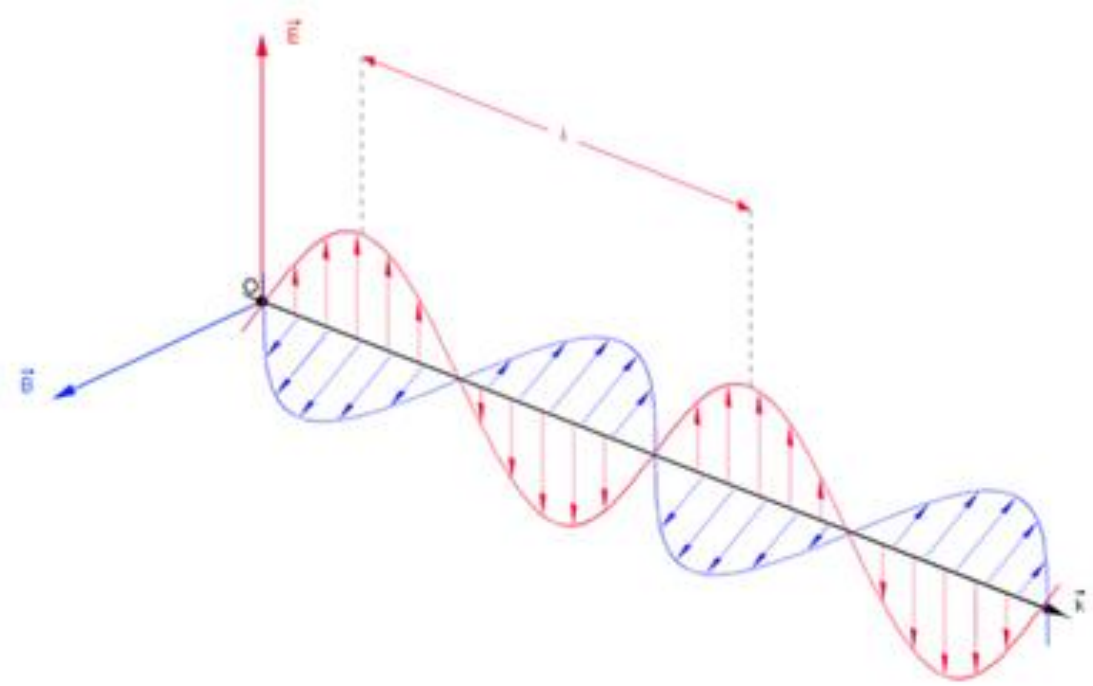

**Figure 2.8 Electromagnetic waves**

Generally, as a wave's wavelength increases, the frequency decreases, and vice versa. When electromagnetic energy is therefore released, as the energy level increases, the wavelength and frequency decreases, which therefore categorises electromagnetic radiation into groups, based on its wavelength or frequency into the electromagnetic spectrum. The different types of electromagnetic radiation shown in the electromagnetic spectrum consist of radio waves, microwaves, infrared waves, visible light, ultraviolet radiation, x-rays and gamma rays.

Ultraviolet, rdiation, x-rays and gamma rays are all related to events occurring in space. UV radiation is the one most commonly known, because of its severe effects on the human skin from the sun, leading to cancer. X-rays are used to produce medical images of the body. Gamma rays can be used in chemotherapy in order to treat tumours in the human body, since it has such a high energy level. The shortest waves,

gamma rays, are approximately $10^{-12}$ m in wavelength. Out of this huge spectrum, the human eye can only detect waves from 390 nm to 780 nm.

Electromagnetic radiation comes in two flavours: near-field and far-field. The intensity of low-frequency radiation drops quickly as a person moves further away from the base station. In other words, the far-field radiation that propagates out in all directions is not very strong at low frequencies, hence is essentially useless. (Wi-fi signals, in comparison, are able to remain strong for tens of meters because they operate at a higher frequency of 2.4 gigahertz.) However, the near-field radiation, which stays close to the base station, contains quite a bit of energy. This bound-up energy, which extends for a couple of meters, is extracted when a resonant receiver on a gadget comes within range.

Electromagnetic radiation can transfer energy over multiple kilometre ranges by means of far-field methods. In some cases, the transfer distance will exceed the diameter of the device. The longer ranges obtained with radio wave and optical devices are due to the fact that electromagnetic radiation in the far-field can be produced to match the shape of the collecting area. This is achieved by using high directivity antennas, which are limited by the diffraction process, as well as well-collimated laser beams that will ensure that almost all the emitted power will be delivered over long ranges.

The dimensions of these devices and lasers will be determined by the distance from the transmitter to the receiver, the wavelength and finally the Rayleigh criterion or diffraction limit that is used in standard radio frequency antenna design. In addition to the Rayleigh criterion that dictates that a radio wave, microwave or laser beam will

diffuse over a certain distance, Airy's diffraction limit can also be used to determine an approximate spot size at an arbitrary distance from the aperture [6].

In this chapter the technology of Wireless Power Transmission (WPT) was discussed, and it was theoretically proven that electrical power can be transmitted wirelessly through inductive coupling over short ranges, and by using resonant inductive coupling through medium ranges.

The theory of resonant inductive coupling will therefore be used as the main technology in the design and implementation of a wireless charging system that can be successfully implemented with AGVs.

Chapter 3

# Wireless power transfer system

*Wireless power transfer is a technology that can transmit power to locations that are not normally possible to reach. The objective of this chapter is to obtain the most effective coil configuration, and to design and implement a system to show the development process of all the components that configures the "Wireless power transfer system". To improve the comprehension on the theories related to "magnetic resonant coupling", quality factor and optimisation techniques, or wireless power transfer systems, a design will be presented, along with the working principles and constructions of various components.*

## 3.1 Introduction

Magnetic coupling is a well-known method in the field of wireless power transfer, and although the magnetic field decays very quickly, it remains effective, but only at very short distances. However, when resonance is applied together with magnetic coupling, power transfer at greater distances can be achieved. In the case of near-field wireless power transfer, magnetic resonant coupling assists in the efficient transfer of energy by "tunnelling" the magnetic field to the receiving coil, which resonates at the same frequency and proves that this method remains one of the most effective methods available. The block diagram for a typical wireless power transfer configuration is shown below. It consists of an AC source, rectifier, oscillator, transmitter, secondary sources and a load [6].

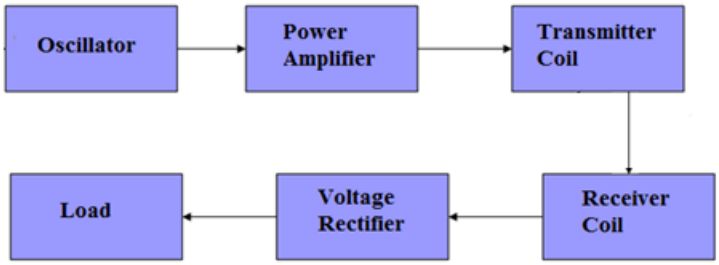


**Figure 3.1 Block diagram of the wireless power transfer system**

The intention is to be able to wirelessly transform and transfer an alternating oscillating waveform into a DC voltage, to demonstrate instantaneous power transfer.

## 3.2 Design of the wireless power system

Figure 3.1 illustrates the components that complete a wireless power transfer system. Wireless power transmission works on the same principle as a transformer. A primary coil is charged, the magnetic flux is generated, and the transformer's core, as well as the secondary core of the transformer, is magnetised. A voltage is induced in the secondary coil of the transformer. The only difference in wireless power transmission is that there is no core between the primary and secondary windings. The importance of the most effective coil configuration that operates without a core can therefore not be overstressed.

The design criteria and performance parameters for each system as indicated in Figure 3.1, should be designed in order to present a suitable charging system for a 3000 mAh metal hydrate battery.

### 3.2.1 **Oscillator**

The frequency oscillator is the device that will generate the magnetic field that allows the coupling circuit to exchange energy. The two main classes of oscillating circuits are relaxation and sinusoidal. Relaxation Op-Amp oscillator uses an RC circuit that produces a current source, which in turn charges and discharges a capacitor and threshold device that induces oscillation. The sinusoidal Op-Amp oscillators operate with a combination of positive and negative feedback that drives the Op-Amp into an unstable state, and causes the output to transition back and forth at a continuous rate.

Oscillators are frequency wave generators that use either active or passive AC components to generate a multitude of waves based on their specific configuration. The two types of passive (LC) oscillators available are Hartley and Colpitts oscillators, specifically selected for their low power consumption.

### 3.2.1.1 Hartley oscillator

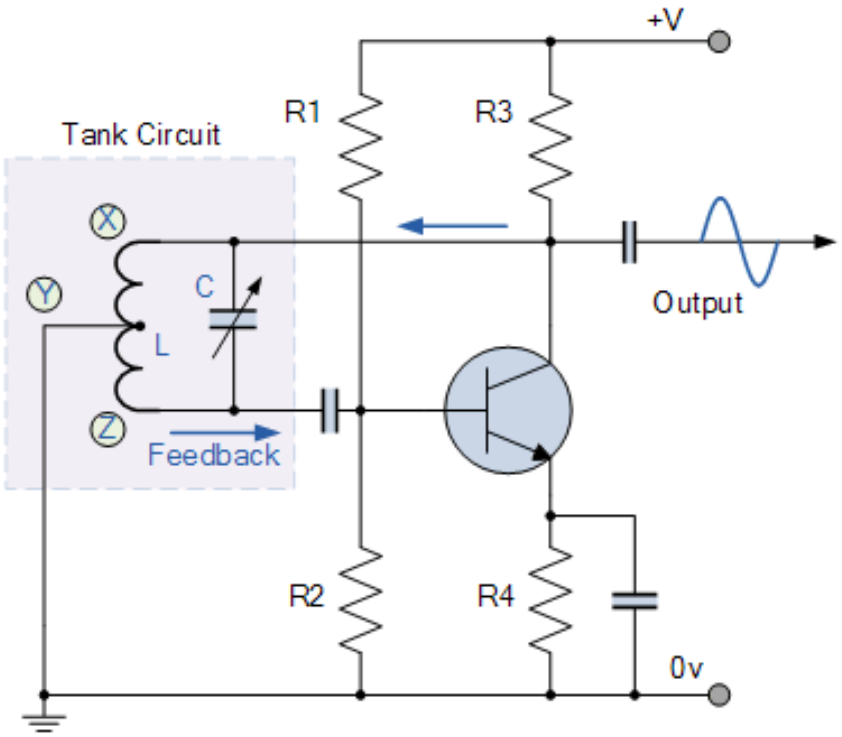


**Figure 3.2 Configuration of the Hartley oscillator**

The basic principle of the Hartley oscillator is the functioning of the commonly referred tank circuit, where a capacitor is placed in parallel with either two separate inductors or a centre tapped inductor. The output frequency can then be achieved from either the centre tap or the middle of the two connected inductors.

When the circuit is oscillating, the voltage at point X (collector), relative to point Y (emitter), is 180˚ out-of-phase with the voltage at point Z (base) relative to point Y. At the frequency of oscillation, the impedance of the collector load is resistive, and an increase in base voltage causes a decrease in the collector voltage.

This results in a 180˚ phase change in the voltage between the base and collector, and along with the original 180˚ phase shift in the feedback loop provides the correct phase relationship of positive feedback for oscillations to be maintained.

The amount of feedback depends upon the position of the “tapping point” of the inductor. If this is moved nearer to the collector, the amount of feedback is increased, but the output taken between the collector and earth is reduced, and vice versa. Resistors R1 and R2 provide the usual stabilising DC bias for the transistor in the normal manner, while the capacitors act as DC-blocking capacitors [9].

### 3.2.1.2 Colpitts oscillator

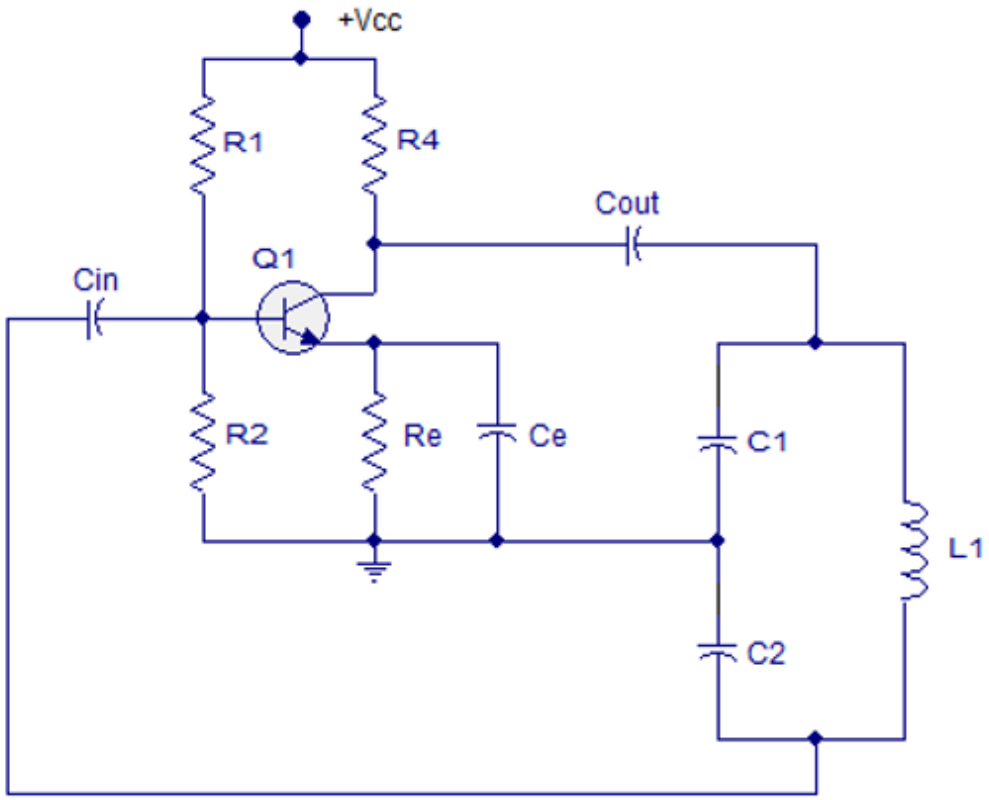


**Figure 3.3 A typical Colpitts oscillator with a transistor on which our design will be based**

The Colpitts oscillator is in a way the exact opposite of the Hartley oscillator. In the Hartley oscillator a centre-tapped inductive circuit is used, whilst a divided capacitive circuit with a parallel inductor is used in the Colpitts oscillator. A Colpitts oscillator uses a capacitive voltage divider as a voltage feedback to the main circuit, where the circuit will begin to oscillate when XC1 + XC2 = XL.

One advantage of the Colpitts oscillator, compared to the Hartley oscillator, is the tendency of the Hartley oscillator to create more mutual and self-conductance, making the theoretical oscillation frequency inaccurate when compared to the physical value. Hence, the Colpitts oscillator is a more improved and stable design.

Collpitts oscillators are normally used in RF applications that range from 20 kHz to 300 MHz. In this circuit the tank consists of two series capacitors connected in parallel with an inductor. The value of the components in the tank determines the frequency of the oscillations. The capacitive voltage divider setup of the Colpitts oscillator works as a feedback source which produces an increased frequency stability, when compared to some of the other arrangements that use inductive voltage division for feedback.

The main advantage of the Colpitts oscillator is found with the improved performance in the high frequency region. The capacitors provide a path of low reactance for the high frequency signals; therefore, the output signals will be more sinusoidal [10].

### 3.2.2 **Power amplifier**

In order to obtain the maximum amount of flux which would induce the maximum voltage on the transmitting coil, a high current has to be transferred into the transmitting coil. An oscillator is not a device that is designed to deliver a great amount of current, hence, the signal from the oscillator has to pass through a power amplifier capable of generating enough current, while producing a clean output signal without large harmonic distortions. Therefore switch-mode power amplifier technology was selected due to the fact that it drives the MOSFET into saturation to switch either the voltage or the current [11].

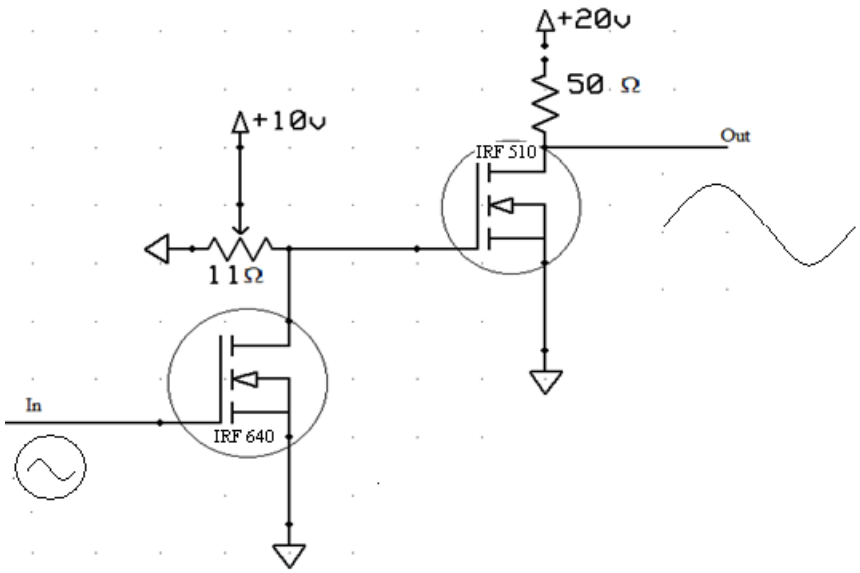


**Figure 3.4 Switch-mode amplifier**

### 3.2.3 Transmitter and receiver coil configuration

The heart of any wireless charging system is the combination of the transmitter and receiver coils, also known as the coupling circuit. The efficiency of this circuit will determine the exact amount of power that will be available for the receiving system. Therefore, it is imperative to establish the most effective coil configuration before the final design phase.

A number of different experimental procedures will be evaluated with respect to the radius, number of windings and thickness of the conductor to establish the effect that these factors will have on the efficiency of power transfer between coils. The results will indicate the best coil configuration for wireless power transfer technology. In all the experiments the final efficiencies will be calculated by obtaining the output power of a secondary coil with respect to the input power at a primary coil. A frequency generator connected to an amplifier will be used to power the circuit, to obtain results for the different configurations.

### 3.2.4 Composition of the inductance of a coil

Inductance is typified by the behaviour of a coil in the resistance that it holds to any change of electrical current through the coil. Although the inductance of a coil depends on the configuration of the coil, as well as the size of the wire and the number of turns, the heart of the inductor remains the shape, size and material of the core. Mechanically the core provides support for the windings, and magnetically the core provides the medium that concentrates and contains the magnetic flux. The combination of winding turns and volume of magnetic material establishes an upper limit on the maximum allowable magnetic flux that a core can sustain. Flux density is of real importance, because it is related to energy. Thus, higher flux densities will result in greater amounts of stored energy.

Another important core parameter is called permeability, which is inversely proportional to the reluctance of the material. A high reluctance produces a low permeability, and vice versa. The importance of permeability cannot be over-emphasised, as it can be seen as a flux multiplier, which in turn leads to a higher inductance. Core permeability is always relative to the permeability of free space, thus the practical values of relative permeability of most magnetic materials ranges from 100 to 1000 [12].

The three types of inductor cores that are available are air-core, iron-core and plate-core inductors. Due to the physical construction features of the three inductors, we will only focus on the plate-core inductor, as this would be the most suitable way of transferring energy between the primary and secondary coils of the wireless charging system for the AGVs.

### 3.2.5 Voltage rectifier

The final section of the circuit consists of a normal full wave bridge rectifier to transform the AC voltage received from the receiving coil to drive the DC battery-operated load. The

single-phase rectifier consists of four individual rectifying diodes that are connected in a closed loop “bridge” configuration that produces the desired output. A smoothing capacitor is normally connected to the bridge circuit to convert the full-wave rippled output of the rectifier into a smooth DC output voltage. Figure 3.9 shows an example of a normal full wave bridge rectifier, with fast signalling diodes that are normally used when Megahertz frequencies are rectified.

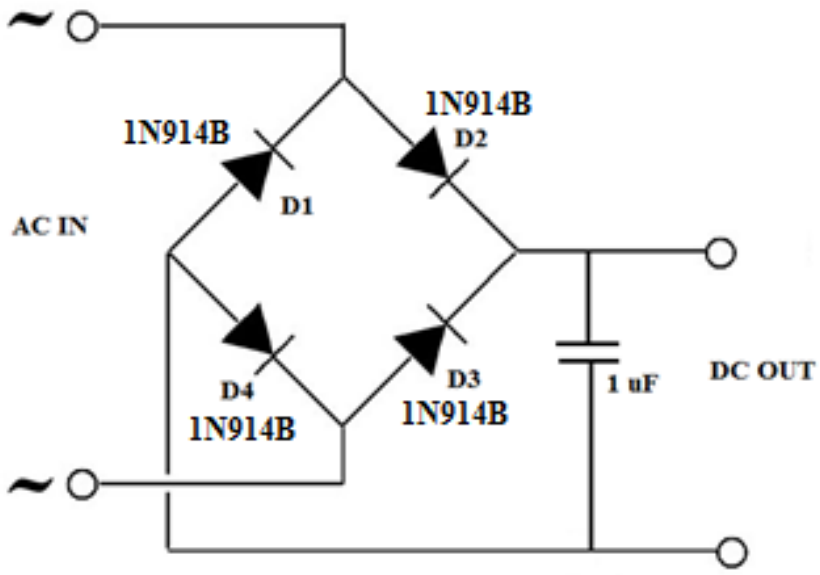


**Figure 3.5 Normal full wave bridge rectifier**

The primary goal in this chapter was to investigate and identify the ideal combination of components as indicated in Figure 3.1, in order to be used in the design and set-up of the wireless power transfer system to be used as a power source to the automatic guided vehicles.

Chapter 4

# Experimental set-up and results

*This chapter covers the initial experiments that was completed to establish the optimum coil configuration that will be used in the wireless power transfer set-up, as well as all the results obtained from the use of these two coils in the complete experimental test set-up for purposes of establishing a resonant wireless power transfer system.*

## 4.1 Experimental procedures for optimum coil configuration

In order to establish the optimum coil configuration, three different coil configurations were prepared by using the same diameter and length of material. The configuration of the three coils, namely a single-layer helix wounded, a single-layer flat-spiral wounded, and a multi-layer flat-spiral was prepared. All three coils were constructed by using 0.45 $mm^2$ copper wire with an identical length of 4 084 mm. The radius used on the single layer helix and the flat spiral was 65 mm, with 20 windings each, while the length of the wire used on the multi-layer flat spiral, was the same as 20 windings of the other two coils. The three different coil configurations are shown in Figure 4.1 below.

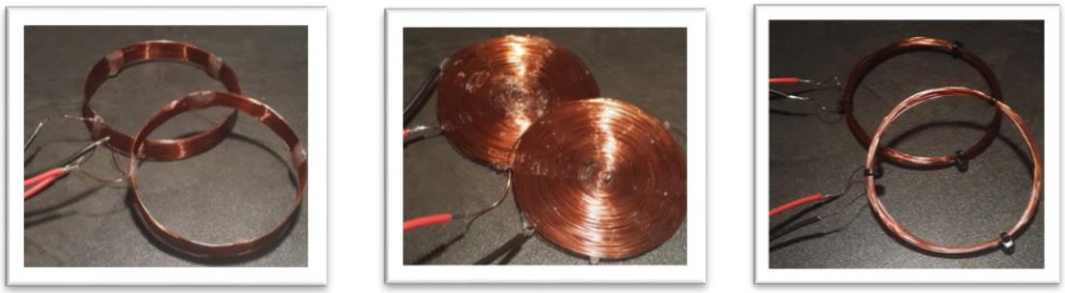

a. b. c.

**Figure 4.1 Single-layer helix (a) Single-layer flat spiral (b) Multi-layer spiral (c)**

Finite Element Method Magnetics (FEMM) software was used to simulate the different coil types, namely the single-layer helix, and single-layer flat spiral, in order to compare the magnetic flux lines and density [13]. The single-layer helix and the multi-layer spiral coil configurations produced similar magnetic field patterns. Hence, it was decided to compare only the multi-layer spiral and single-layer flat spiral with the use of the software. The magnetic flux lines of the different coils and the pattern of the fields can easily be observed. Graphs were compiled with the position of the red line indicating the magnetic field strength at specific positions in the magnetic field. A horizontal and a vertical graph were drawn to observe the magnetic field strength of the coil.

The simulation was run with an input current to the coils of 5A. The supply frequency was kept constant at 100 Hz. Each coil had 10 windings and was made of 2.5 mm copper wire.

**Single-layer helix**

The cross section of a single-layer helix coil drawn in FEMM software can be observed in Figure 4.2 below. The coil had 10 windings, with the negative sign as an indication of the direction of the coil windings, thus 10 winding into the page, and 10 winding out of the page. The medium between the coils is air. The coil is made out of 2.5 $mm^2$ copper wire.

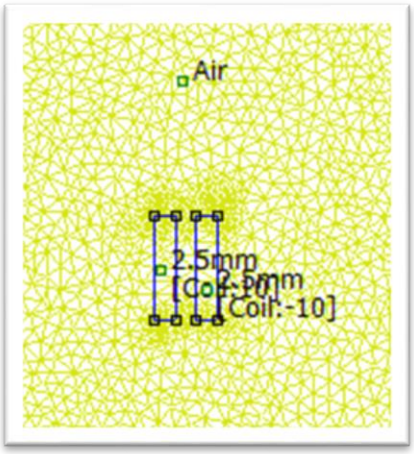


**Figure 4.2 A single-layer helix coil drawn in FEMM software**

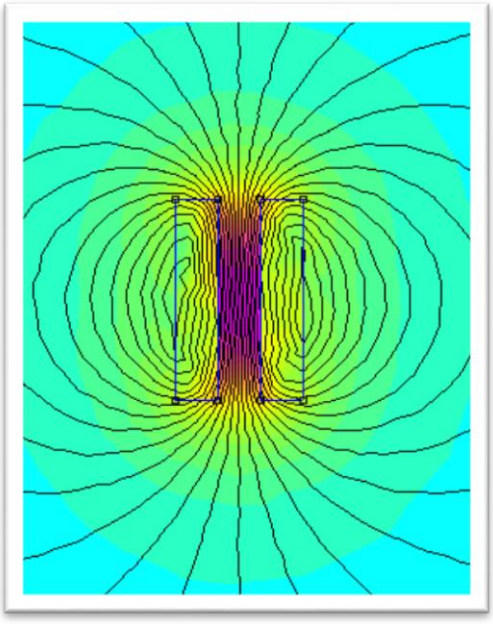

**Figure 4.3 The flux density and magnetic lines of a single-layer helix coil, represented as a colour density plot**

The cross-section area of a single-layer helix coil is observed in Figure 4.3. The colours indicate the strength of the magnetic field, with the higher intensity colour presenting a stronger magnetic field. The lines indicate the shape of the magnetic field formed.

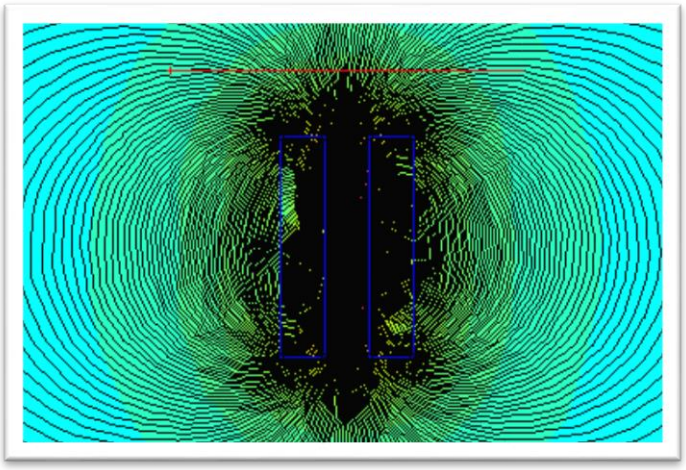

**Figure 4.4 The flux density and magnetic lines of a single-layer helix coil, horizontal to the coil**

The position of the red line shown in Figure 4.4 produces the graph as shown below in Figure 4.5. This graph represents the flux density horizontal to the coil. It shows that the magnetic field strength is the strongest closest to the coil, and it weakens as the distance increases away from the coil.

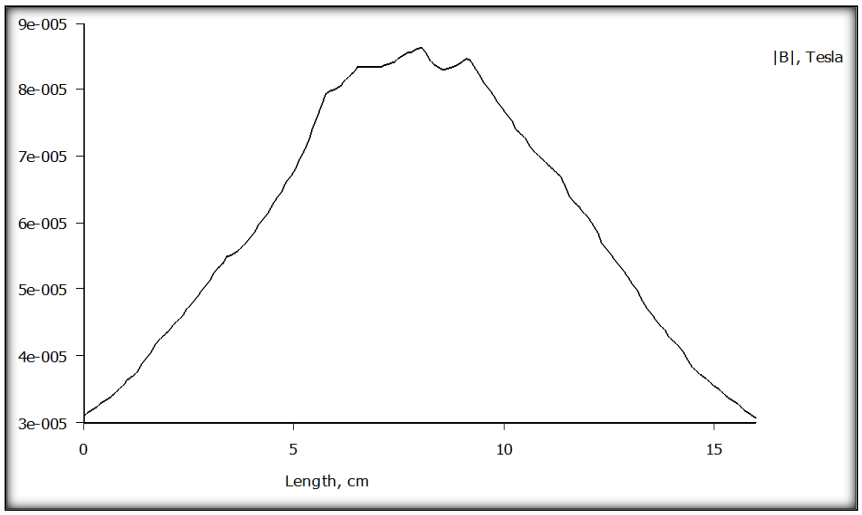


**Figure 4.5 The graph shows the distance versus the magnetic field strength in Tesla**

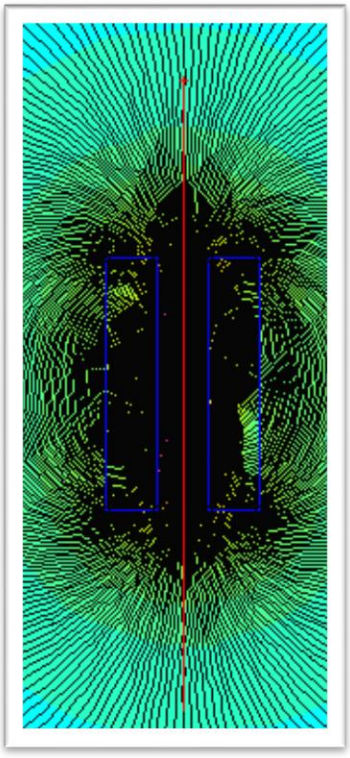

**Figure 4.6 The flux density and magnetic lines of a single-layer helix coil, vertical to the coil**

The position of the red line shown in Figure 4.6 produces the graph as shown below. Figure 4.7 indicates the flux density drawn vertical to the coil, and it can be observed that the magnetic field strength increases to the centre of the coil. As the distance increases away from the coil, the magnetic field strength weakens.

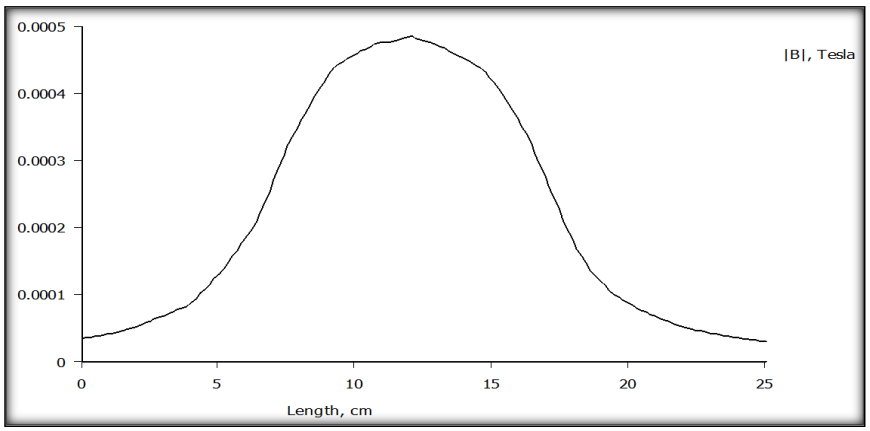


**Figure 4.7 The graph shows the magnetic field strength versus distance**

### Single-layer flat spiral

The cross section of a single flat spiral coil drawn in FEMM software is shown in Figure 4.8. The coil had 10 windings, with the negative sign as an indication of the direction of the coil windings, thus 10 winding into the page, and 10 winding out of the page. The medium between the coils is air. The coil is made out of 2.5 $mm^2$ copper wire.

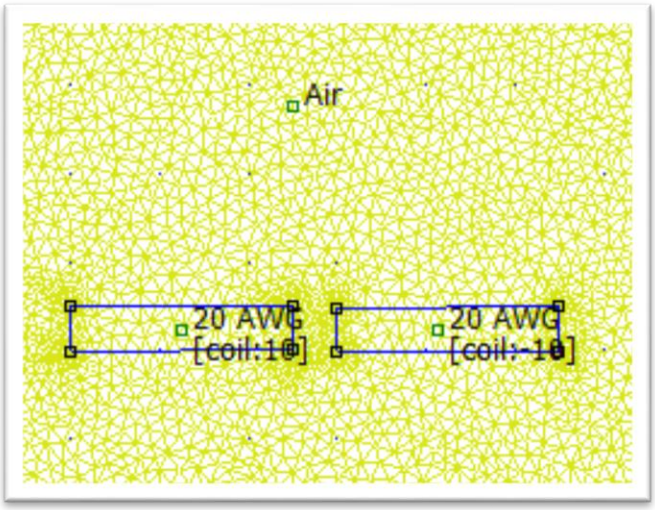


**Figure 4.8 A single-layer flat spiral coil drawn in FEMM software**

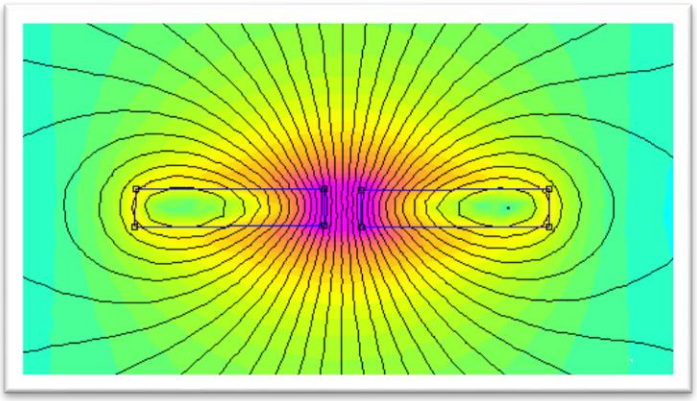

**Figure 4.9 The black lines are an indication of the magnetic flux lines when current flows through the coil**

The basic flux lines of the coil can be observed in Figure 4.9, which indicates how circles are formed around the conductors of the coil. The different colours show the strength of the magnetic flux density of the coil. The magnetic fields are strong in the centre of the coil, and weaken away from the coil.

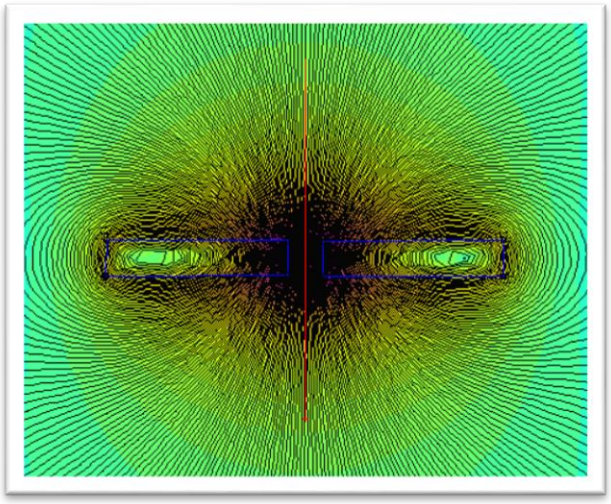

**Figure 4.10 The flux density and magnetic lines of a single-layer flat spiral coil, vertical to the coil**

The position of the red line shown in Figure 4.10 produces the graph shown below, drawn vertical to the coil.

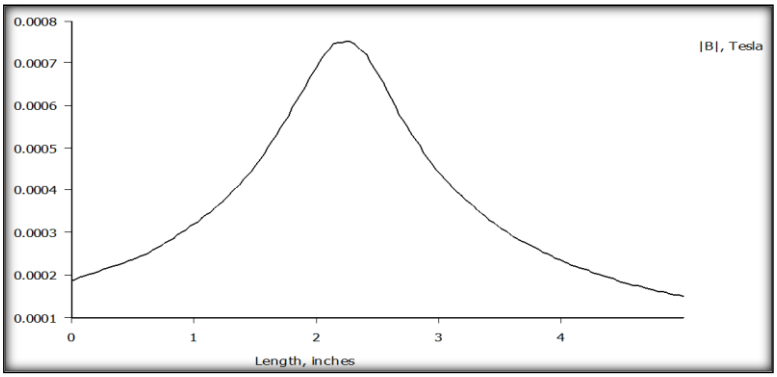


**Figure 4.11 The graph shows the distance versus the magnetic field strength in Tesla**

The magnetic field strength is the strongest closest to the coil, and it weakens as the distance increase away from the coil. Figure 4.11 indicates the flux density drawn vertical to the

coil, and it can be observed that the magnetic field strength increases to the centre of the coil. As the distance increases away from the coil, the magnetic field strength weakens.

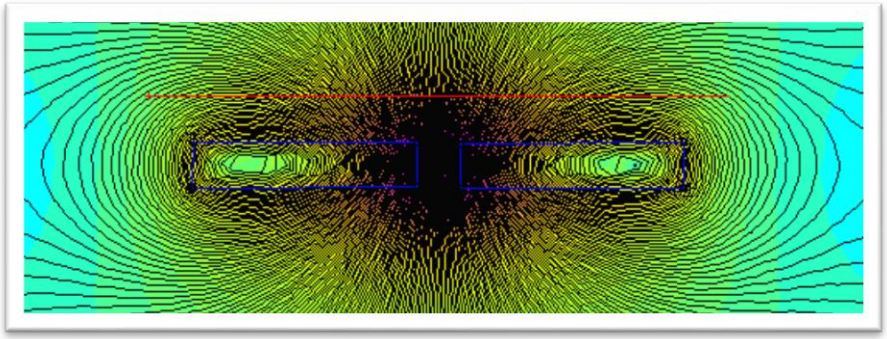

**Figure 4.12 The flux density and magnetic lines of a single-layer flat spiral coil, horizontal to the coil**

The position of the red line shown in Figure 4.12 produces the graph shown below, drawn horizontal to the coil.

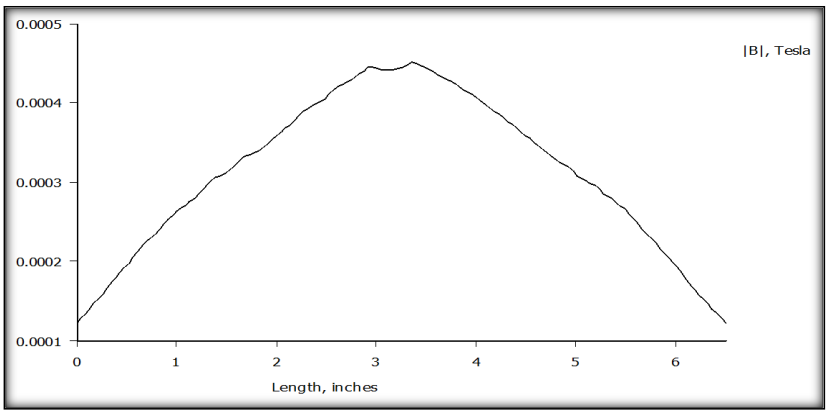


**Figure 4.13 The graph shows the distance versus the magnetic field strength of the horizontal line**

The magnetic field strength is the strongest closest to the coil, and it weakens as the distance increase away from the coil. Figure 4.13 indicates the flux density drawn vertical to the coil, and it can be observed that the magnetic field strength increases to the centre of the coil. As the distance increases away from the coil, the magnetic field strength weakens.

### 4.1.1 Evaluation for optimum coil configuration

A number of different experimental procedures were completed with respect to the radius, number of windings and thickness of the conductor to establish the effect that these had on the efficiency of power transfer between coils. The results will be used to establish the best coil configuration for wireless power transfer technology. In all the experiments the final efficiencies were calculated by obtaining the output power of a secondary coil with respect to the input power at a primary coil, as shown in equation 19.

$$N(efficiency) = \frac{Output\ secondary\ power}{Input\ primary\ power} \tag{19}$$

A frequency generator connected to an amplifier was used to power the circuit that was used to obtain results for the different configurations.

In the first experiment the normal efficiencies were obtained, with readings at intervals of 10 mm from 0 - 50 mm.

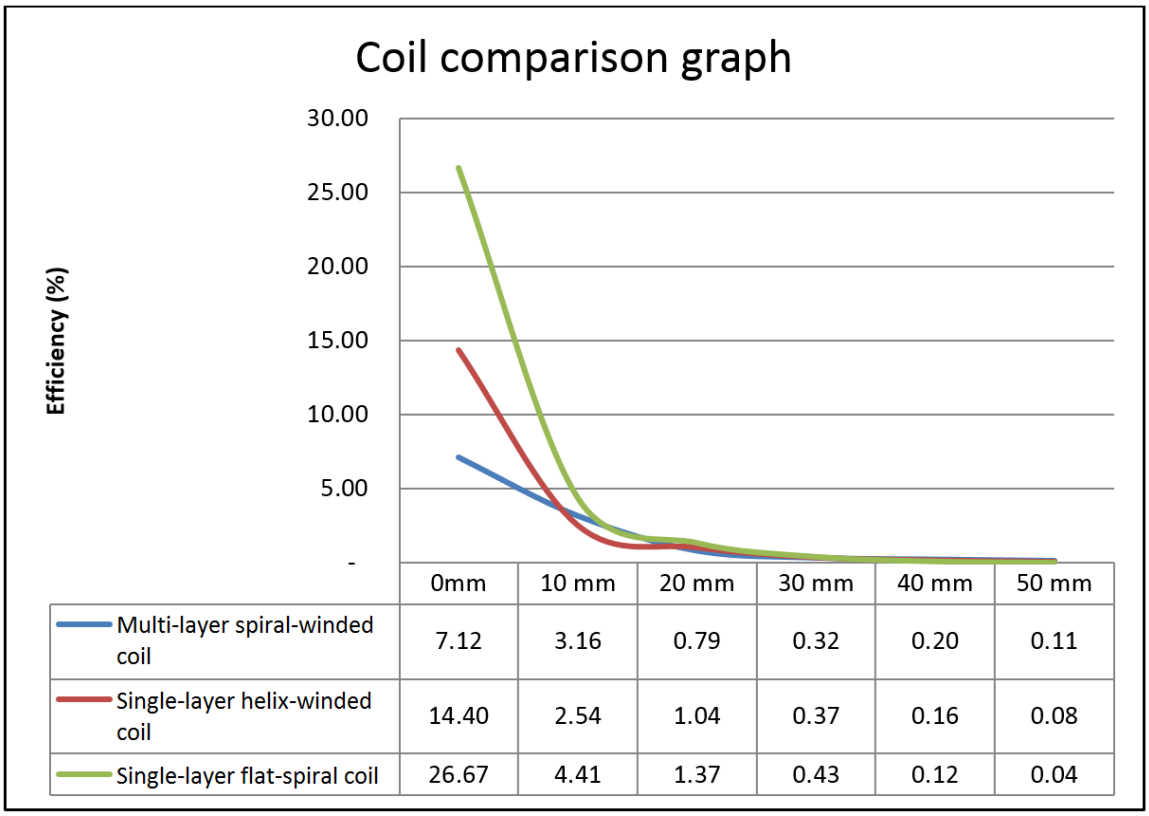


**Figure 4.14 Efficiencies of the three coil configurations**

Although it is common knowledge that the efficiency of any coil configuration is reduced when the distance between the coils is increased, the results show that the single-layer flat-spiral wounded coil has the best efficiency.

In the second experiment the frequencies applied were increased from 100 Hz – 10 kHz to obtain the maximum power transfer point, otherwise known as the resonant frequency.

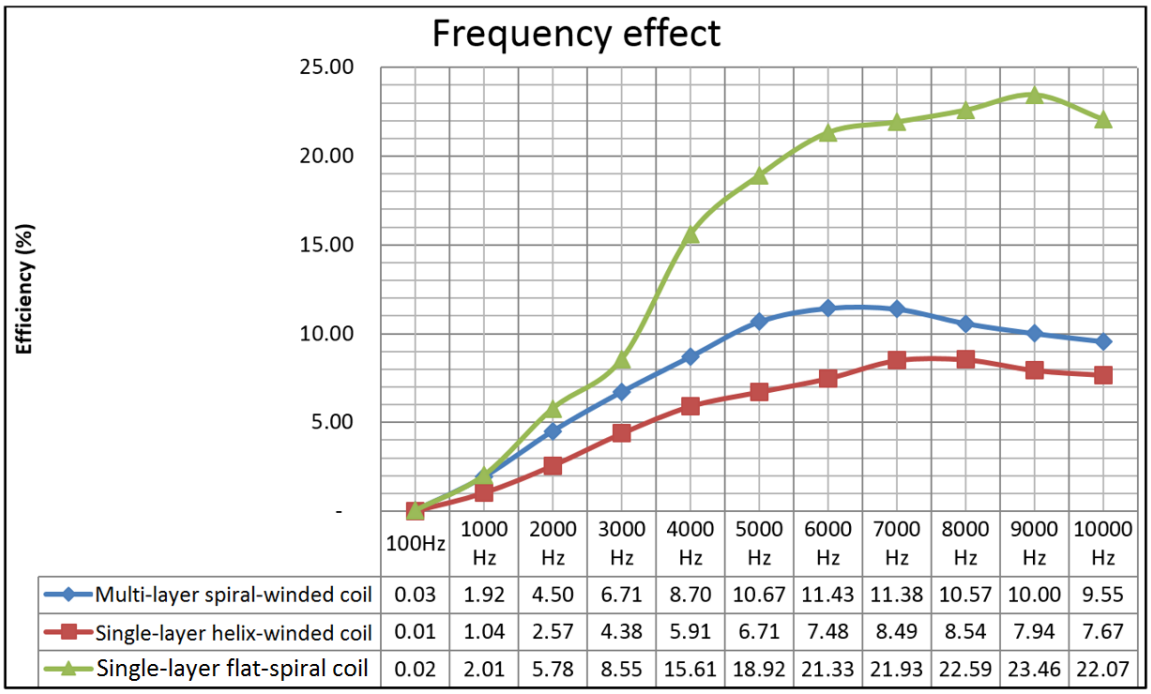


**Figure 4.15 Maximum power transfer point or resonant frequency point**

Maximum power transfer occurs at resonant frequencies. The graph indicates that with similar coil configurations, the power transfer with the flat-spiral wounded coil has the best efficiency.

The aim of the third experiment was to establish how the angle at which the two coils are aligned affects the maximum power transfer between the coils.

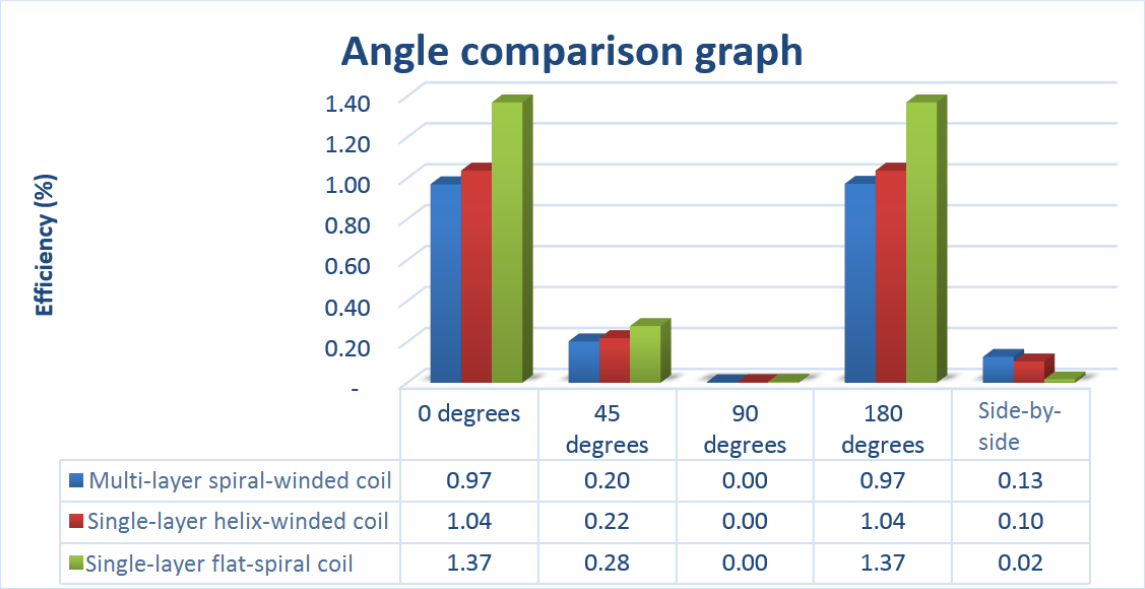


| | 0 degrees | 45 degrees | 90 degrees | 180 degrees | Side-by-side |
|---|---|---|---|---|---|
| Multi-layer spiral-winded coil | 0.97 | 0.20 | 0.00 | 0.97 | 0.13 |
| Single-layer helix-winded coil | 1.04 | 0.22 | 0.00 | 1.04 | 0.10 |
| Single-layer flat-spiral coil | 1.37 | 0.28 | 0.00 | 1.37 | 0.02 |

**Figure 4.16 Alignment effect between the two coils**

The results of all three simulations indicate that the single-layer flat-spiral-winded coil configuration achieves the best efficiency. The results obtained from these simulations will be applied in the subsequent design of the coupling circuit.

### 4.1.2 Experimental test set-up

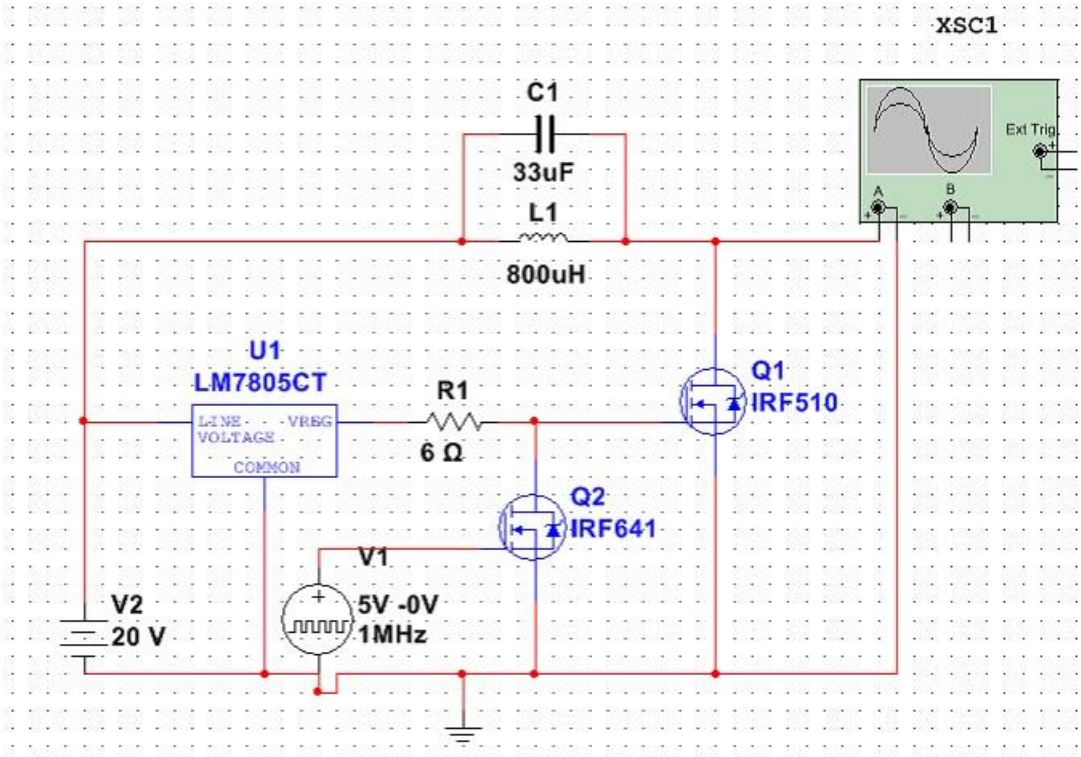


**Figure 4.17 Experimental set-up with Multisim software**

The figure above shows the Multisim software used to simulate the simple circuit to test the different coil configurations [14]. It involves LM7805 in parallel with a 20V DC supply. The LM7805 will then regulate the voltage to feed the digital on signal of the IRF510. However, once the square wave Colpitts oscillator triggers the IRF610 MOSFET, an easier ground path is taken from the output of the LM7805 regulator, switching off the IRF510 MOSFET. On the other half of the parallel connection of the 20V DC supply is the LC network with the primary inductor coil. Once the IRF510 is switched on, it creates a path to ground for the current to flow through the inductor. However, with the constant switching of the IRF510 between states, this creates an AC-like signal of a square wave from 0-20 volts. The parallel capacitor connected over the inductor will assist in obtaining a resonant

circuit, therefore reducing the amount of impedance and increasing the amount of current that flows through the coil and therefore increasing the electromagnetic field strength.

Different configurations with respect to the resistance, capacitance and constant inductance were completed, and with the optimal circuit selected the voltage fall-off was measured across some distances. The table below shows the values obtained, and proves that the voltage measured on the secondary side should be sufficient to charge the battery of the wireless-connected charging circuit.

**Table 4.1 Output voltage versus distance configurations**

| Distance (cm): | Output (Volts): |
|---|---|
| 20 | 45 |
| 30 | 38 |
| 40 | 18 |
| 50 | 10 |
| 60 | 8 |
| 70 | 6 |

Although the MOSFETS, coupled with the Colpitts oscillator design, offers a highly efficient system, the distance covered by the electro-magnetic field rapidly decreases with an exponential factor.

The following formula as shown in equation 19 shows the reduction in magnetic field strength of an inductor with respect to distance:

$$B_{axis} = \frac{\mu_o \, 2\mu}{4\pi d^3} \quad (19)$$

Where:

$B_{axis}$ = the magnetic field (measured in Tesla);

$\mu_o$ = the permeability constant ($4\pi \times 10^{-7}$ T m /A);

$\mu$ = magnetic moment; and

d = distance from the centre of the dipole in meters.

The maximum power transfer characteristics are greatly increased through impedance matching, on the primary and secondary coils, as well are greatly dependent on the electromagnetic field, which can be strengthened by either increasing the maximum current through the coil, or by increasing the inductance rating of the coil.

### 4.1.3 **Final test set-up and recorded results**

The efficiency of the coupling circuit determines the amount of power available for the receiving load. The parameters of the two coils that configure the coupling circuit were determined by the practical implementation and design of the secondary coil. The theoretical model and circuit implementation of the wireless charging system for the AGV was based on the actual dimensions of the AGV, as well as the charging requirements of the 3000 mAh Nickel Metal Hydrate battery that is used to drive the AGV. Although the coil configuration was based on the charging requirements of the battery, the output power generated at the secondary coil will always be limited by the input power from the source. The evaluation of the optimum coil configuration conducted in paragraph 4.1.1 indicated that the flat, regularly-spaced conductor is not only the most suitable application, but it also

proved to have the highest efficiency, and therefore it was selected as the secondary winding to be implemented on the AGV. The basic configuration of the design can be seen from the table and images below.

**Table 4.2 Primary and secondary coil specifications**

| | Primary coil | Secondary coil |
|---|---|---|
| Conductor Ø | 0.5 mm | 0.32 mm |
| Current rating | 5.2 A | 3.4 A |
| Coil inner Ø | 36 mm | 21 mm |
| Coil outer Ø | 152 mm | 119 mm |
| L without lamination | 16.53 mH | 26.56 mH |
| L with lamination | 30.53 mH | 40.11 mH |

The conductor material used for the two coils was silver-plated copper with polyvinylidene fluoride (PVDF). Both coils are rated at 300 V.

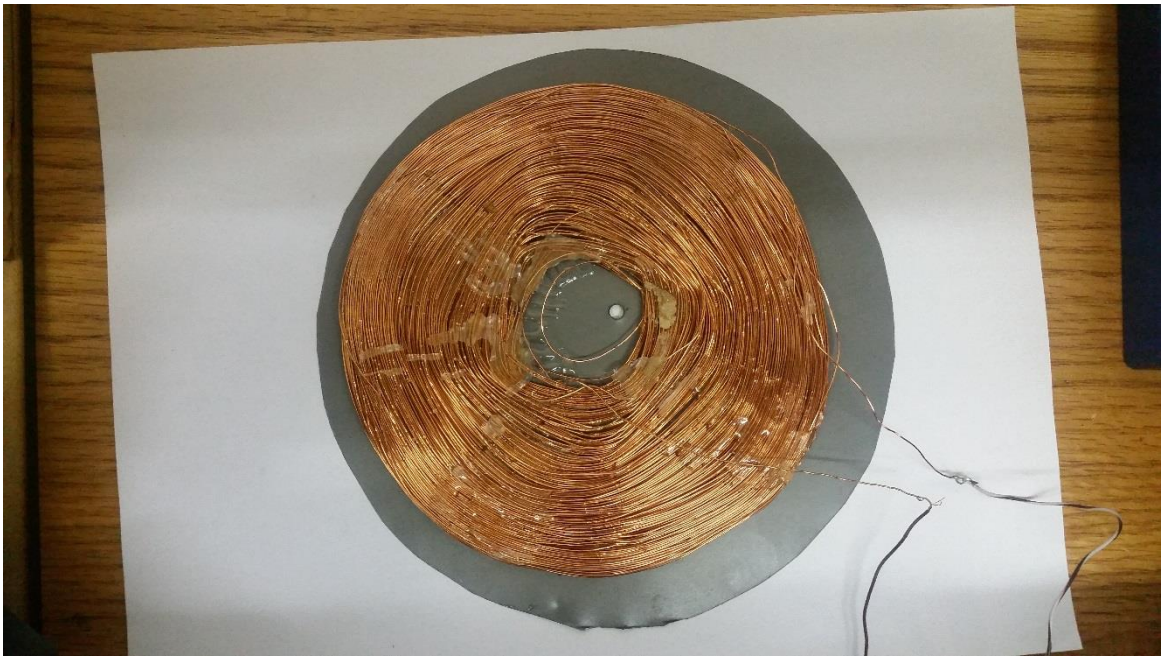

**Figure 4.18 Primary coil on laminated core**

**Figure 4.19 Secondary coil on laminated core**

The lamination material used in both coils is transformer-laminated silicon steel, with a density of 7.65 kg/m³, and a core loss rating of 1.1 W/kg, obtained from Free State Transformers, a local supplier. Effective use of lamination is of utmost importance to improve the inductance, as seen in Table 4.2.


**Figure 4.20 Hardboard mould with 5 mm increments for the coils**

A hardboard mould as shown in Figure 4.20, was designed and manufactured by means of a laser cutting process, in order to assist with the final testing procedures.

A preliminary test was completed in order to record the inductance value of both coils at 1 kHz, with increments of 5 mm between 0 and 100 mm, to determine the effect of the mutual inductance between the two coils.

**Table 4.3 Inductance test on both coils at 1 kHz sine wave**

| Distance(mm) | Coil A (mH) | Coil B (mH) |
|---|---|---|
| **Stand-alone** | **30.53** | **40.11** |
| 0 | 51.33 | 65.59 |
| 5 | 44.66 | 57.62 |
| 10 | 39.15 | 52.02 |
| 15 | 36.62 | 47.87 |
| 20 | 34.59 | 45.18 |
| 25 | 33.18 | 43.55 |
| 30 | 32.47 | 42.36 |
| 35 | 31.77 | 41.65 |
| 40 | 31.42 | 41.08 |
| 45 | 31.1 | 40.74 |
| 50 | 31.05 | 40.56 |
| 55 | 30.84 | 40.38 |
| 60 | 30.7 | 40.22 |
| 65 | 30.64 | 40.2 |
| 70 | 30.58 | 40.16 |
| 75 | 30.53 | 40.12 |
| 80 | 30.52 | 40.11 |
| 85 | 30.45 | 40.09 |
| 90 | 30.45 | 40.06 |
| 95 | 30.43 | 40.03 |
| 100 | 30.42 | 40.03 |

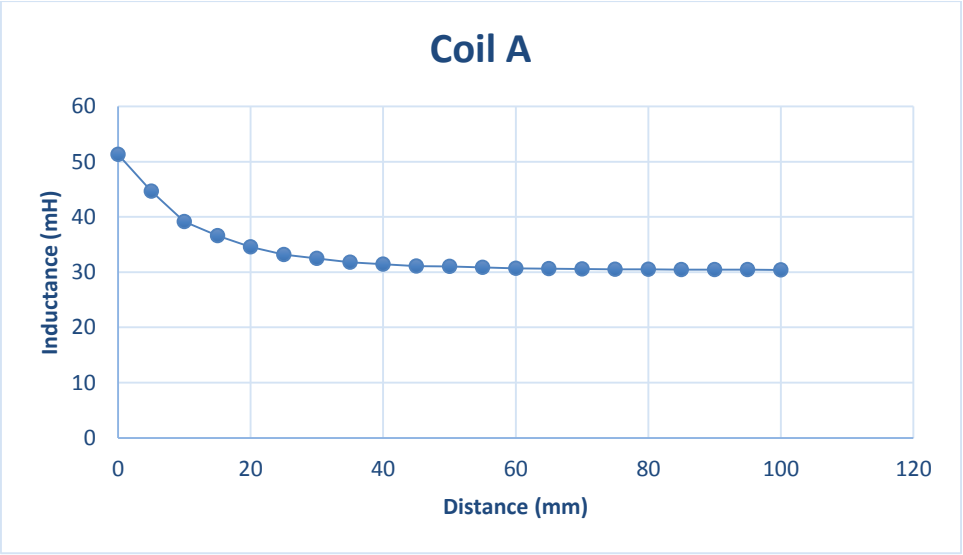


**Figure 4.21 Recorded variation of inductance of coil A**

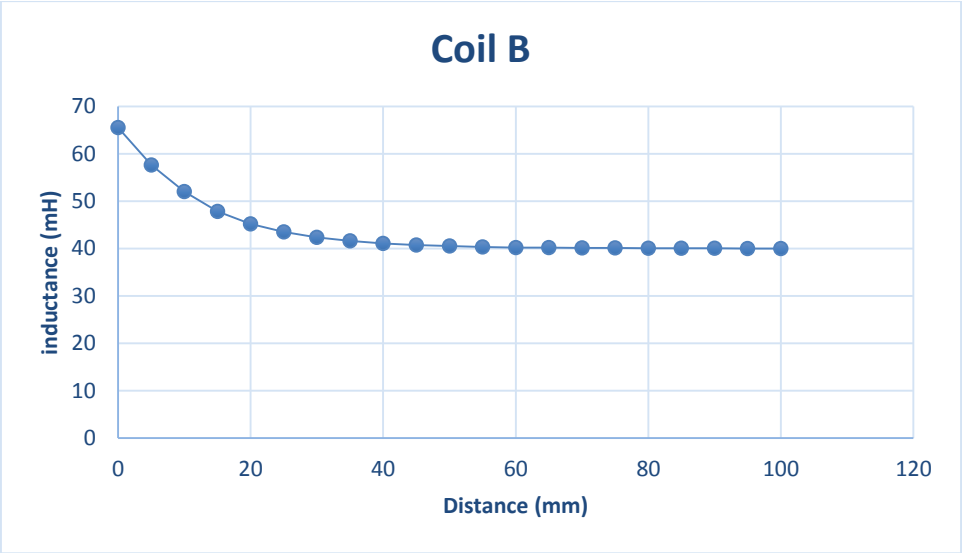


**Figure 4.22 Recorded variation of inductance of coil B**

It is evident from Figure 4.21 and Figure 4.22 that the mutual inductance between the two coils is negligible from a distance between the two coils of 50 mm and further.

The final two testing procedures, was done by changing the distance between the two coils with increments of 5 mm. The first set of results was obtained without any load connected to the secondary supply, and the second set of results was obtained with a 10 kΩ load resistor connected to the secondary supply. The purpose of the tests was to obtain the resonant frequency at each increment, and to record the input and output power parameters. The values recorded were the input (DC) voltage and current, the oscillated (AC) voltages across both the coils, as well as the rectified output (DC) voltage and current through the load.

In Figure 4.23 the practical test set-up is shown that was applied to all the different recorded values. In Table 4.4 the resonant frequency can clearly be seen to be approximately 1100 Hz, with the generated DC voltage at 14. 2 Volt.

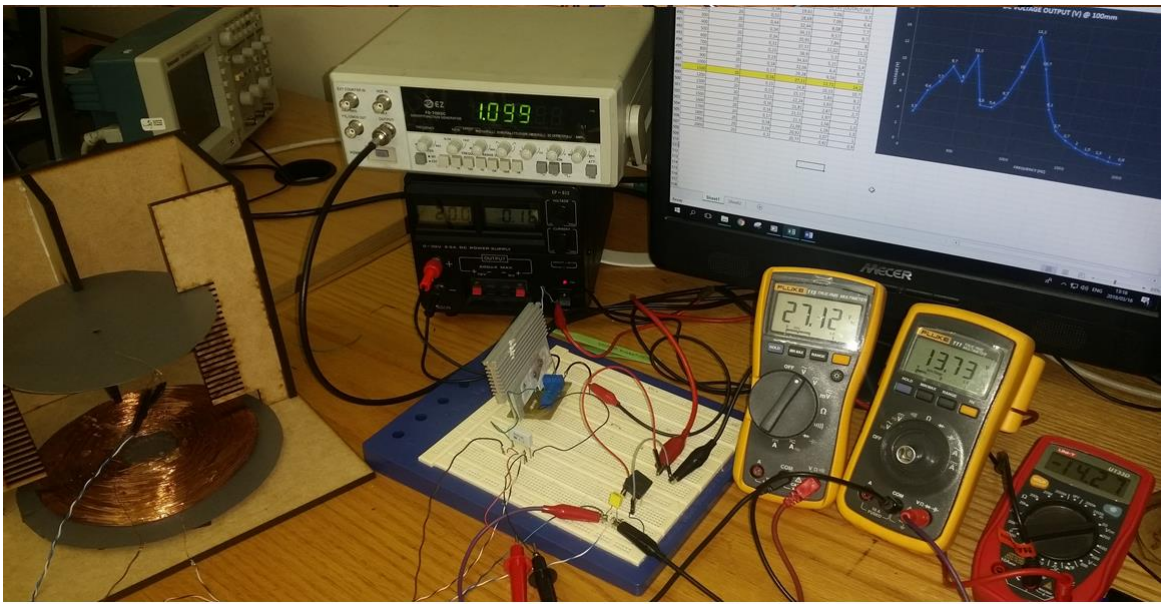


**Figure 4.23 Practical test set-up with coils 100 mm apart and no load**

**Table 4.4 Recorded test results with coils 100 mm apart and no load**

| EFFECT OF FREQUENCY WITH NO LOAD @ 100mm | | | | | |
|---|---|---|---|---|---|
| FREQUENCY (HZ) | INPUT VOLTAGE (DC) | INPUT CURRENT (A) | COIL A VOLTAGE (AC) | COIL B VOLTAGE (AC) | VOLTAGE OUTPUT (DC ) |
| 100 | 20 | 0.58 | 19.61 | 5.06 | 3.7 |
| 200 | 20 | 0.51 | 28.69 | 7.09 | 6.4 |
| 300 | 20 | 0.44 | 32.44 | 8.08 | 7.7 |
| 400 | 20 | 0.34 | 34.11 | 9.57 | 9.7 |
| 500 | 20 | 0.34 | 35.91 | 7.84 | 8 |
| 600 | 20 | 0.31 | 37.37 | 11.02 | 11.3 |
| 700 | 20 | 0.23 | 36.9 | 5.3 | 5.5 |
| 800 | 20 | 0.19 | 34.63 | 5.21 | 5.4 |
| 900 | 20 | 0.18 | 32.06 | 6.4 | 6.7 |
| 1000 | 20 | 0.17 | 29.28 | 9.59 | 10 |
| 1100 | 20 | 0.16 | 27.11 | 13.71 | 14.2 |
| 1200 | 20 | 0.15 | 24.8 | 10.33 | 10.7 |
| 1300 | 20 | 0.15 | 23.17 | 5.83 | 6.1 |
| 1400 | 20 | 0.15 | 22.24 | 3.63 | 3.7 |
| 1500 | 20 | 0.16 | 21.81 | 2.67 | 2.7 |
| 1600 | 20 | 0.16 | 21.51 | 1.97 | 2 |
| 1700 | 20 | 0.17 | 21.3 | 1.56 | 1.5 |
| 1800 | 20 | 0.18 | 21.09 | 1.29 | 1.3 |
| 1900 | 20 | 0.19 | 20.92 | 1.07 | 1 |
| 2000 | 20 | 0.2 | 20.77 | 0.92 | 0.9 |

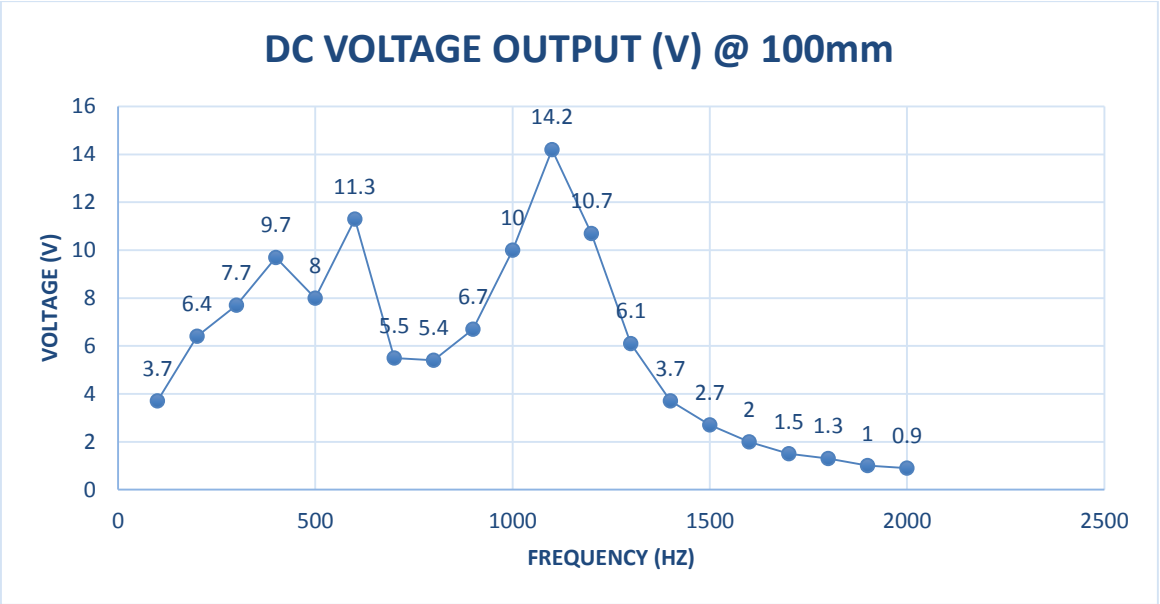


**Figure 4.24 Recorded DC voltage at coils 100 mm apart with no load**

The following table and graph depict the recorded values with the same set-up and two coils 100 mm apart, with a load resistor of 10 kΩ connected to the circuit.

**Table 4.5 Recorded test results with coils 100 mm apart and a 10 kΩ load resistor**

| EFFECT OF FREQUENCY WITH 10kΩ LOAD @ 100mm | | | | | | |
|---|---|---|---|---|---|---|
| FREQUENCY (HZ) | INPUT VOLTAGE (DC) | INPUT CRRENT (A) | COIL A VOLTAGE (AC) | COIL B VOLTAGE (AC) | VOLTAGE OUTPUT (DC) | CALCULATED CURRENT (mA) |
| 100 | 20 | 0.61 | 20.19 | 4.78 | 2.1 | 0.21 |
| 200 | 20 | 0.51 | 25.61 | 6.88 | 4.3 | 0.43 |
| 300 | 20 | 0.44 | 31.91 | 7.9 | 5.2 | 0.52 |
| 400 | 20 | 0.35 | 33.75 | 9.64 | 7.2 | 0.72 |
| 500 | 20 | 0.34 | 35.9 | 8.45 | 6.3 | 0.63 |
| 600 | 20 | 0.31 | 37.04 | 8.86 | 6.5 | 0.65 |
| 700 | 20 | 0.25 | 36.66 | 5.38 | 3.6 | 0.36 |
| 800 | 20 | 0.19 | 34.85 | 5.19 | 3.7 | 0.37 |
| 900 | 20 | 0.18 | 32.19 | 6.49 | 4.6 | 0.46 |
| 1000 | 20 | 0.17 | 29.49 | 8.91 | 6.9 | 0.69 |
| 1100 | 20 | 0.16 | 27.12 | 12.22 | 9.8 | 0.98 |
| 1200 | 20 | 0.16 | 25.11 | 9.83 | 7.7 | 0.77 |
| 1300 | 20 | 0.15 | 23.27 | 5.73 | 4.2 | 0.42 |
| 1400 | 20 | 0.15 | 22.3 | 3.6 | 2.3 | 0.23 |
| 1500 | 20 | 0.16 | 21.82 | 2.54 | 1.4 | 0.14 |
| 1600 | 20 | 0.17 | 21.54 | 1.94 | 0.9 | 0.09 |
| 1700 | 20 | 0.17 | 21.35 | 1.58 | 0.7 | 0.07 |
| 1800 | 20 | 0.18 | 21.16 | 1.3 | 0.4 | 0.04 |
| 1900 | 20 | 0.19 | 20.95 | 1.06 | 0.3 | 0.03 |
| 2000 | 20 | 0.2 | 20.77 | 0.9 | 0.2 | 0.02 |

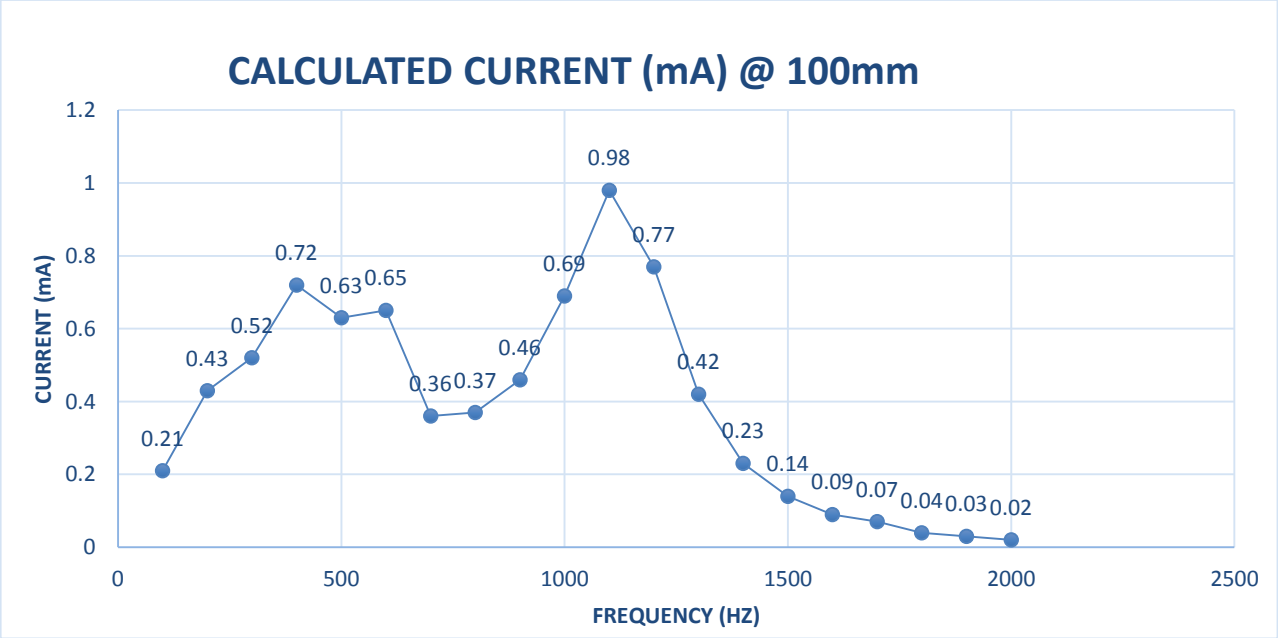


**Figure 4.25 Calculated current with coils at 100mm and load of 10 kΩ**

The recorded values for the increments at 50 mm and 10 mm are shown in the tables and graphs below.

**Table 4.6 Recorded test results with coils 50 mm apart and no load**

| EFFECT OF FREQUENCY WITH NO LOAD @ 50mm | | | | | |
|---|---|---|---|---|---|
| FREQUENCY (HZ) | INPUT DC VOLTAGE (V) | INPUT CURRENT (A) | COIL A AC VOLTAGE (V) | COIL B AC VOLTAGE (V) | DC VOLTAGE OUTPUT (V) |
| 100 | 20 | 0.57 | 19.4 | 17.3 | 12.7 |
| 200 | 20 | 0.51 | 27.8 | 23 | 20.5 |
| 300 | 20 | 0.41 | 31.4 | 25.21 | 23.8 |
| 400 | 20 | 0.4 | 33.4 | 33.52 | 33.8 |
| 500 | 20 | 0.35 | 36.6 | 26.15 | 27.1 |
| 600 | 20 | 0.3 | 35.17 | 36.57 | 37.8 |
| 700 | 20 | 0.25 | 36.78 | 19.14 | 19.8 |
| 800 | 20 | 0.19 | 34.94 | 18.07 | 18.8 |
| 900 | 20 | 0.18 | 31.64 | 21.81 | 22.9 |
| 1000 | 20 | 0.18 | 28.08 | 29.98 | 31.6 |
| 1100 | 20 | 0.2 | 24.51 | 43.97 | 46.3 |
| 1200 | 20 | 0.2 | 25.3 | 40.27 | 42.8 |
| 1300 | 20 | 0.17 | 24.04 | 21.82 | 23.3 |
| 1400 | 20 | 0.16 | 22.7 | 14.1 | 15 |
| 1500 | 20 | 0.16 | 21.97 | 9.8 | 10.3 |
| 1600 | 20 | 0.16 | 21.59 | 7.41 | 7.7 |
| 1700 | 20 | 0.17 | 21.33 | 5.59 | 6 |
| 1800 | 20 | 0.18 | 21.14 | 4.64 | 4.9 |
| 1900 | 20 | 0.18 | 20.96 | 3.86 | 4.1 |
| 2000 | 20 | 0.19 | 20.78 | 3.29 | 3.5 |

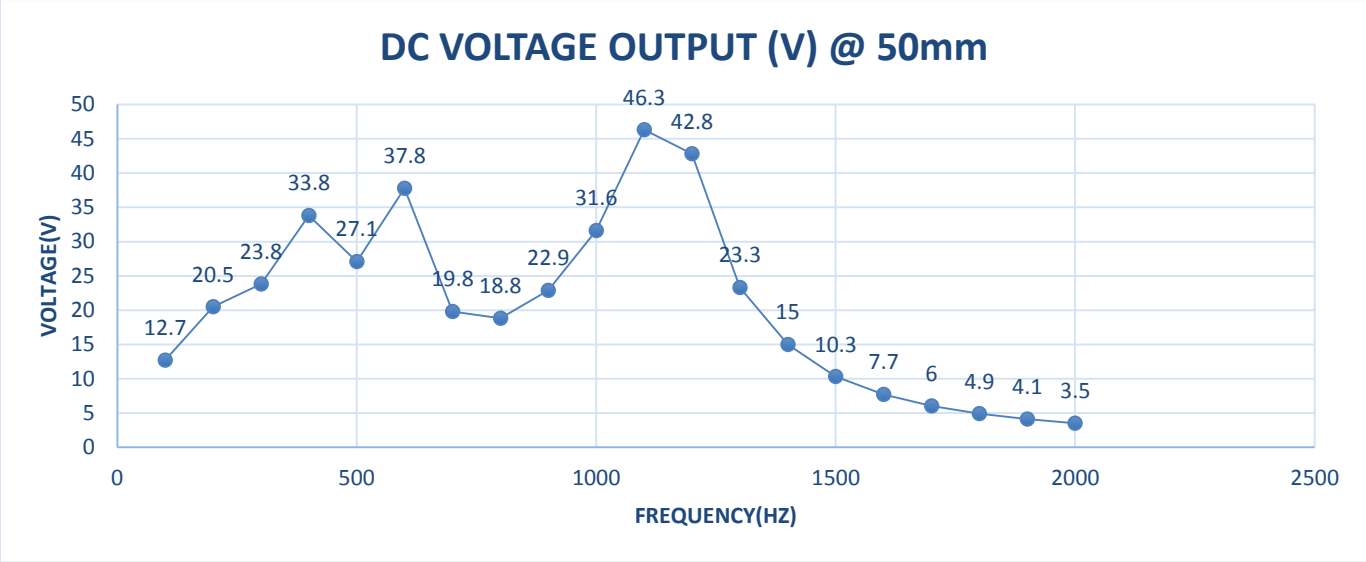


**Figure 4.26 Recorded DC voltage at coils 50 mm apart with no load**

**Table 4.7 Recorded test results with coils 50 mm apart and a 10 kΩ load resistor**

| EFFECT OF FREQUENCY WITH 10KΩ LOAD @ 50mm | | | | | | |
|---|---|---|---|---|---|---|
| FREQUENCY (HZ) | INPUT VOLTAGE (DC) | INPUT CURRENT (A) | COIL A VOLTAGE (AC) | COIL B VOLTAGE (AC) | VOLTAGE OUTPUT (DC) | CALCULATED CURRENT (mA) |
| 100 | 20 | 0.6 | 20.18 | 15.96 | 8.4 | 0.84 |
| 200 | 20 | 0.5 | 27.49 | 20.91 | 14.6 | 1.46 |
| 300 | 20 | 0.42 | 20.82 | 23.27 | 16.6 | 1.66 |
| 400 | 20 | 0.38 | 33.29 | 27.31 | 21.9 | 2.19 |
| 500 | 20 | 0.35 | 35.57 | 27.03 | 22.3 | 2.23 |
| 600 | 20 | 0.31 | 35.04 | 32.37 | 26.6 | 2.66 |
| 700 | 20 | 0.25 | 36.51 | 18.24 | 14 | 1.4 |
| 800 | 20 | 0.2 | 35.33 | 17.51 | 14.3 | 1.43 |
| 900 | 20 | 0.18 | 31.87 | 20.66 | 17.3 | 1.73 |
| 1000 | 20 | 0.18 | 27.84 | 27.76 | 23.6 | 2.36 |
| 1100 | 20 | 0.2 | 25.05 | 39.61 | 34.2 | 3.42 |
| 1200 | 20 | 0.2 | 25.18 | 35.21 | 30.3 | 3.03 |
| 1300 | 20 | 0.17 | 23.9 | 20.79 | 17.4 | 1.74 |
| 1400 | 20 | 0.16 | 22.64 | 13.34 | 10.8 | 1.08 |
| 1500 | 20 | 0.16 | 21.93 | 9.33 | 7.3 | 0.73 |
| 1600 | 20 | 0.16 | 21.57 | 7.15 | 5.3 | 0.53 |
| 1700 | 20 | 0.17 | 21.32 | 5.43 | 4 | 0.4 |
| 1800 | 20 | 0.18 | 21.12 | 4.5 | 3.2 | 0.32 |
| 1900 | 20 | 0.19 | 20.93 | 3.17 | 2.5 | 0.25 |
| 2000 | 20 | 0.19 | 20.77 | 3.23 | 2.1 | 0.21 |

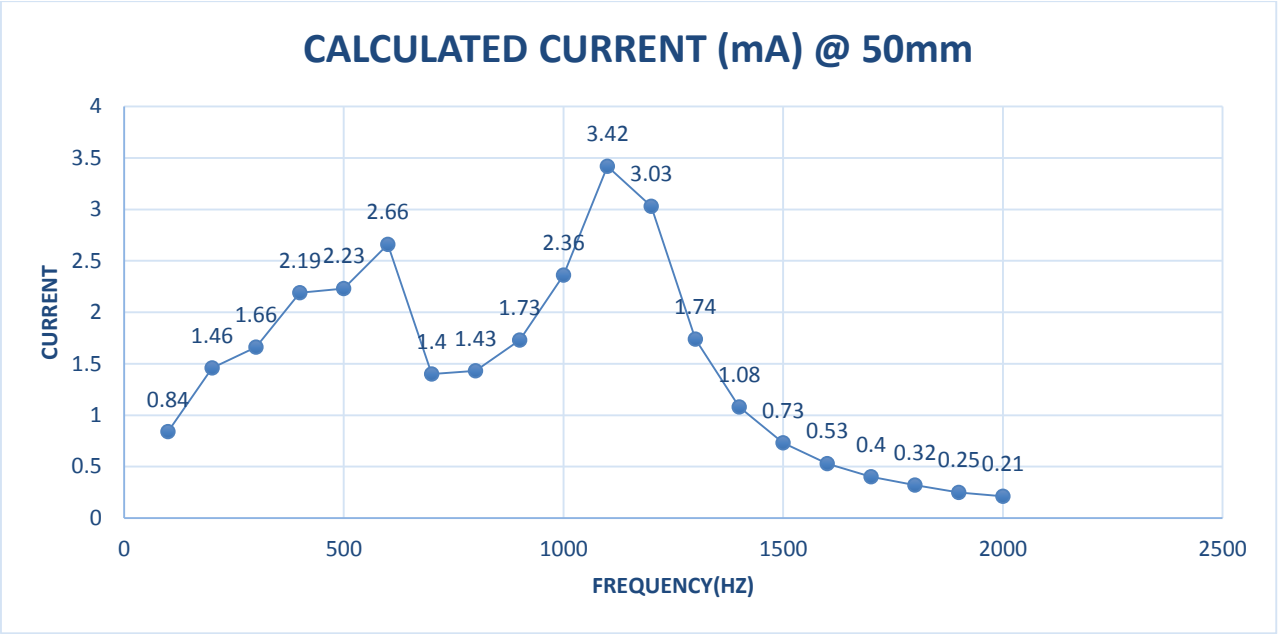


**Figure 4.27 Calculated current with coils at 50 mm and load of 10 kΩ**

**Table 4.8 Recorded test results with coils 10 mm apart and no load**

| EFFECT OF FREQUENCY WITH NO LOAD @ 10mm | | | | | |
|---|---|---|---|---|---|
| FREQUENCY (HZ) | INPUT VOLTAGE (DC) | INPUT CURRENT (A) | COIL A VOLTAGE (AC) | COIL B VOLTAGE (AC) | VOLTAGE OUTPUT (V) |
| 100 | 20 | 0.54 | 19.79 | 27.2 | 16.5 |
| 200 | 20 | 0.45 | 17.1 | 38.06 | 29.7 |
| 300 | 20 | 0.36 | 30.66 | 43.12 | 38 |
| 400 | 20 | 0.31 | 32.2 | 46.06 | 41.8 |
| 500 | 20 | 0.23 | 30.7 | 39.88 | 38.8 |
| 600 | 20 | 0.19 | 25.61 | 33.7 | 34 |
| 700 | 20 | 0.17 | 22.5 | 28.68 | 29.2 |
| 800 | 20 | 0.18 | 22.15 | 30.46 | 32.8 |
| 900 | 20 | 0.18 | 21.71 | 38.16 | 41.6 |
| 1000 | 20 | 0.23 | 21.6 | 48.07 | 51.8 |
| 1100 | 20 | 0.3 | 19.75 | 55.63 | 60.1 |
| 1200 | 20 | 0.36 | 16.87 | 62.5 | 68.1 |
| 1300 | 20 | 0.43 | 17.7 | 70.4 | 78.1 |
| 1400 | 20 | 0.42 | 24.14 | 66.5 | 74.7 |
| 1500 | 20 | 0.32 | 25.49 | 51.43 | 57.9 |
| 1600 | 20 | 0.24 | 24.46 | 35.8 | 40.4 |
| 1700 | 20 | 0.2 | 23.35 | 27.35 | 30.8 |
| 1800 | 20 | 0.18 | 22.19 | 21.44 | 24.1 |
| 1900 | 20 | 0.18 | 21.43 | 17.19 | 19.3 |
| 2000 | 20 | 0.18 | 20.96 | 13.95 | 15.7 |

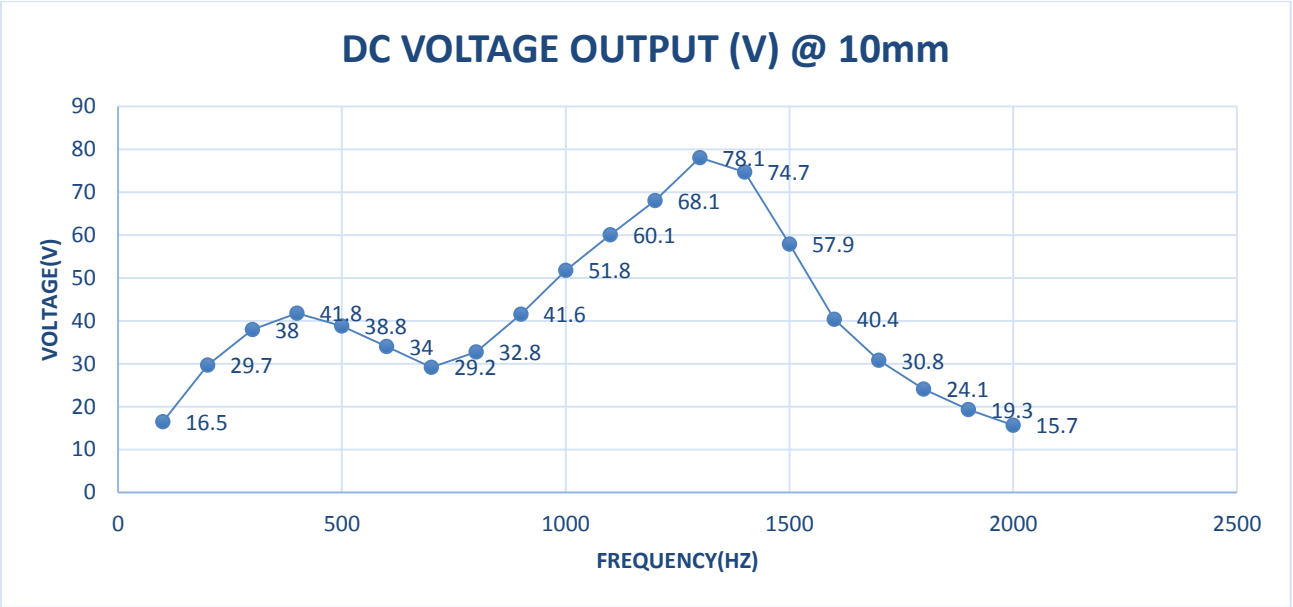


**Figure 4.28 Recorded DC voltage at coils at 10 mm apart with no load**

**Table 4.9 Recorded test results with coils 10 mm apart and a 10 kΩ load resistor**

| EFFECT OF FREQUENCY WITH 10 kΩ LOAD @ 10mm | | | | | | |
|---|---|---|---|---|---|---|
| FREQUENCY (HZ) | INPUT VOLTAGE (DC) | INPUT CURRENT (A) | COIL A VOLTAGE (AC) | COIL B VOLTAGE (AC) | VOLTAGE OUTPUT (DC) | CALCULATED CURRENT (mA) |
| 100 | 20 | 0.55 | 21.44 | 30.15 | 11.7 | 1.17 |
| 200 | 20 | 0.44 | 29.34 | 42.16 | 22.7 | 2.27 |
| 300 | 20 | 0.35 | 31.12 | 43.53 | 26.5 | 2.65 |
| 400 | 20 | 0.31 | 32.25 | 44.44 | 29.7 | 2.97 |
| 500 | 20 | 0.23 | 29.9 | 39.56 | 28.4 | 2.84 |
| 600 | 20 | 0.2 | 25.71 | 33.69 | 25.3 | 2.53 |
| 700 | 20 | 0.17 | 22.08 | 28.75 | 22.5 | 2.25 |
| 800 | 20 | 0.18 | 21.34 | 30.36 | 24.1 | 2.41 |
| 900 | 20 | 0.19 | 21.02 | 37.11 | 31.1 | 3.11 |
| 1000 | 20 | 0.23 | 21.26 | 45.88 | 39.9 | 3.99 |
| 1100 | 20 | 0.3 | 19.82 | 52.66 | 46.1 | 4.61 |
| 1200 | 20 | 0.36 | 17.33 | 58.97 | 51.7 | 5.17 |
| 1300 | 20 | 0.42 | 17.3 | 65.2 | 57.6 | 5.76 |
| 1400 | 20 | 0.43 | 21.66 | 65.5 | 57.8 | 5.78 |
| 1500 | 20 | 0.34 | 24.88 | 51.96 | 45 | 4.5 |
| 1600 | 20 | 0.26 | 24.78 | 39.01 | 33.5 | 3.35 |
| 1700 | 20 | 0.22 | 23.63 | 30.01 | 25.5 | 2.55 |
| 1800 | 20 | 0.19 | 22.44 | 23.82 | 20 | 2 |
| 1900 | 20 | 0.18 | 21.49 | 18.53 | 15.3 | 1.53 |
| 2000 | 20 | 0.18 | 21.07 | 15.79 | 12.9 | 1.29 |

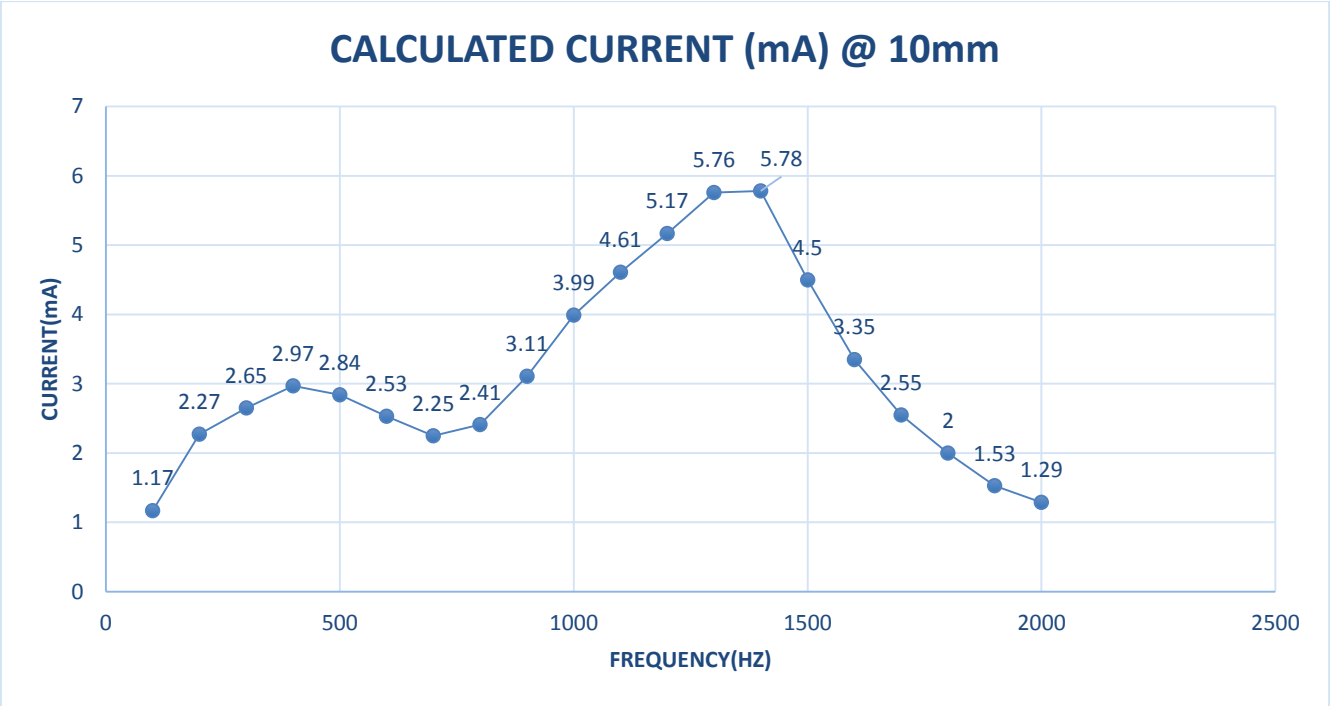


**Figure 4.29 Calculated current with coils at 10 mm and load of 10 kΩ**

A comparison of the efficiencies calculated at resonance in the circuit with the load resistor connected, shows that the overall efficiency between the input AC power and the output DC power increases from 0.5 % with the coils 100 mm apart to 3.58 % with the coils 10 mm apart. Although the results shows that there is a substantial increase in the output power at shorter distances between the coils, is it important to note that the output power generated at resonance, is much higher than the output power generated at any other frequency. This shows that the efficiency of the system depends on the fact that the power transfer should always occur at resonance.

Chapter 5

# Conclusion

*In this chapter the results of the study for a wireless charging system are discussed, and some recommendations are made towards improvement of the overall design.*

## 5.1 Wireless power transmission

This study analyses and designs a wireless power transmission system by means of resonant coupling. It introduces wireless power transmission technology, as well as a combination of traditional coupling and resonance. This study contains the modelling and construction of the hardware to prove the feasibility of wireless power transmission through resonant coupling based on numerical calculation [14]. Experimental results prove that significant improvements in terms of wireless power transfer efficiency have been achieved. Measured results are in good agreement with the theoretical models. It is described and demonstrated that magnetic resonant coupling can be used to deliver power wirelessly from a source coil to a load. The resonant frequency of the coils changes with a change in the air-gap or distance between the coils. Since the maximum power transfer efficiency occurs at resonance, it is important that the resonant frequency is established between the two coils. Despite this significant development, the effective transmission distance will always be limited by the size of the resonator. In many applications it would be highly desirable to extend the distance of transmission, and to allow the route of transmission to follow a curved path in space. Modern approaches reduce the transfer losses with ultra-thin coils,

higher frequencies and improved drive electronics, thus providing chargers and receivers that are compact and far more efficient. These technologies provide charging times that are similar to wired approaches, and are rapidly finding their way into all the different charging devices.

This study also focused on the different coil configurations, and the evaluation of the optimum coil configuration conducted indicated that the flat regularly-spaced conductor is not only the most suitable application, but also proved to have the highest efficiency, and therefore selected as the most suitable secondary winding to be implemented on the AGV.

## 5.2 Future work

This study has established that power can effectively be transmitted through resonant inductive wireless technology. However, the efficiency of such a system can be enhanced with the application of some other technologies.

It is known that the dominant loss in any power transfer system is due to the internal source resistance, whether through wires or through a wireless power transfer system. The high internal resistance of the oscillator can be significantly reduced by using a more practical power source. The use of an intermediate coil positioned close to the source coil will increase the Q-factor to a great extent [15]. The intermediate coil will absorb most of the power from the source coil and then transfer it to the load coil. The Q-factor will be improved due to the fact that the intermediate coil does not have the internal resistance within it. Therefore, the transfer efficiency and the power transfer range will increase significantly [16].

The increased use of electric vehicles requires a safe and convenient method of charging. Studies similar to this paper has provided efficient mid-range wireless power transfer through magnetic resonant coupling, also known as WiTricity. It is known that the resonant frequency varies with a change in the gap between the two coils, and when this technology is applied in the MHz range that produces higher transfer efficiencies, the usable frequency is bounded by the Industrial, Science, and Medical (ISM) band.

Therefore, to achieve maximum power transmission efficiency, the resonant frequency has to be fixed within the ISM band. Impedance matching theory is a technology that uses a specifically designed tuning circuit placed between the source coil and the load coil, to match the impedances and reach a fixed resonant frequency for the two coils [17].

## 5.3 Applications

Power is very important to modern-day systems and appliances, from the smallest sensors, bionic implants, laptops, consumer products, electric vehicles to satellites. Modern science, however, has now made it possible to use electricity without having to plug in any wires for charging. It has been demonstrated that it is feasible to wirelessly transmit a significant amount of power at a high efficiency.

Automatic wireless charging established a new era in consumer electronics with the charging application of mobile electronics, effectively eliminating the use of disposable batteries and awkward charging cables. Direct wireless power and communication systems at points of use in harsh environments, like drilling, mining, and underwater applications, effectively reduce the use of costly and failure-prone wiring.

WiTricity has already greatly impacted the transportation section with the stationary wireless charging of electric vehicles at homes, parking areas, fleet depots and remote kiosks, with future applications to hybrid and all electric passenger, industrial and commercial vehicles. All of these efforts, though, still depend on a vehicle stopping when it needs to recharge. In that sense, wireless charging is no different from the plug-in variety, although for induction to work, the vehicle does not need to be stationary. Therefore, the application of wireless charging technology to vehicles on the move has become the new field of study [18].

# References

[1] *Automated guided vehicles*. N.d. [Online]. Available: http://www.witricity.com. [Accessed 7 August 2013].

[2] *Battery conductor systems*. N.d. [Online]. Available: http://www.vahle.com. [Accessed 14 August 2013].

[3] *Wireless Power*. N.d. [Online]. Available: http://wirelesspowerconsortium.com. [Accessed 7 August 2013].

[4] *Wireless energy transfer*. N.d. [Online]. Available: http://www.mit.edu. [Accessed 28 August 2013].

[5] *Wireless-Electrical-Energy-Transfer*. N.d. [Online]. Available: http://muonry.blogspot.com. [Accessed 20 October 2014].

[6] *Resonant magnetic coupling*. N.d. [Online]. Available: http://www.ijsrp.org. [Accessed 21 August 2013].

[7] *Resonant inductive coupling*. N.d. [Online]. Available: http://www.sciencedirect.com. [Accessed 21 August 2013].

[8] Liu, X., Ng, W., Lee, C. & Hui, S. 2008. Optimal operation of contactless transformers with resonance at secondary circuit. *APEC*, pp. 645-650.

[9] *Hartley Oscillator*". N.d. [Online]. Available: http://www.electronics-tutorials.ws. [Accessed 15 March 2017].

[10] *Colpitts Oscillators*. N.d. [Online]. Available: http://www.electronics-tutorials.ws. [Accessed 10 March 2017].

[11] Sibakoti, M.J. & Hambleton, J. 2011. *Wireless power transmission using magnetic resonance.* [Online]. Available:

http://www.academia.edu/download/34735897/mandip-sibakoti.pdf. [Accessed 10 March 2013].

[12] *Wireless Power*. N.d. [Online]. Available: http://www.powerelectronics.com. [Accessed 8 March 2014].

[13] Meeker, D. 2006. *Finite Element Method Magnetics (FEMM), Version 4.2*.

[14] Veeradasan, P., Azuwa, A., Hashim, U. and Tijjani, A. 2012. Development of Circuit Structure for Near Field Wireless Power Transmission using Resonant Coupling. *Far East Journal of Electronics and Communication 9(2):*99-110.

[15] Jinwook, K., Hyeon-Chang, S., Kwan-Ho, K. and Young-Jin, P. 2011. Efficiency analysis of magnetic resonance wireless power transfer with intermediate resonant coil. *IEEE antennas and wireless propagation letters* 10:389-392.

[16] Gupta, S.D., Shahinur, I., Kawser, N., Hossain, M.S. and Hasan, Z. 2012. Design & Implementation of Cost Effective Wireless Power Transmission Model: GOOD BYE Wires. *International Journal of Scientific and Research Publications* 12(2):1-9.

[17] TeckChuan, B., Masaki, K., Takehiro, I. and Yoichi, H. 2010. Wireless Power Transfer System via Magnetic Resonant Coupling at Fixed Resonance Frequency-Power Transfer System Based on Impedance Matching. *World Electric Vehicle Journal* 4:744-753.

[18] T. Economist. N.d. *"It is now practical te refuel electric vehicles through thin air*" [Online]. Available: http://www.economist.com. [Accessed 28 October 2017].

[19] *Opportunity charging of AGV's*. N.d. [Online]. Available: http://wwwegeminusa.com. [Accessed 7 August 2013].

[20] *Near field and Far field electromagnetic induction*. N.d. [Online]. Available: http://www.W8ji.com. [Accessed 21 August 2013].

[21] *Circuits Today*. N.d. [Online]. Available: http://www.circuitstoday.com. [Accessed 10 February 2015].

[22] Hu, A.P. 2009. *Wireless/Contactless power supply: Inductively coupled resonant convertor solutions.* VDM Verlag: Oxford.

[23] Karalis, A., Joannopoulos, J. and Soljacic, M. 2008. *Efficient wireless non-radiative mid-range energy transfer*. *Annals of Pysics* 323:34-48.

[24] Kurs, A., Karalis, A., Moffat, R., Joannopoulos, J., Fischer, P. and Soljacic, M. 2007. *Wireless power transfer via strongly coupled magnetic resonances. Science* 317(5834):83-86.

[25] Kristopher, C.P. 2007. MIT engineers unveil wireless power system. *Daily Tech.*

[26] Noyes, K. 2007. MIT wizards zap electrically through air. *The Economist.*

[27] Basharat, N. 2013. Inductive Charging Technique. *International Journal of Engineering Trends and Technology (IJETT)* 4(4):1055-1059.

[28] Xing, L.K. and Wang, W.J. 2014. Magnetic coupling resonance system parameters research of wireless power transmission. *Applied Mechanics and Materials* 602:2696-2699.

[29] Li, S. and Chunting, C.M. 2015. Wireless power transfer for electric vehicle applications. *IEEE Journal of Emerging and Selected Topics in Power Electronics* 3(1):4-17